Available online at www.CivileJournal.org

Civil Engineering Journal

(E-ISSN: 2476-3055; ISSN: 2676-6957)

Vol. 10, No. 12, December, 2024

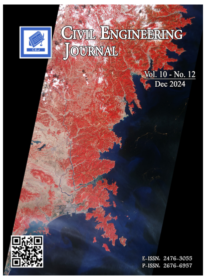

Flexural Performance of a New Composite Double PSSDB Slab System Filled with Recycled Concrete

Zaid A. Al-Sudani [1], Fatimah De'nan [1*], Ahmed W. Al-Zand [2, 3], Noorhazlinda Abd Rahman [1], Mohammed C. Liejy [2, 4]

[1] *School of Civil Engineering, Engineering Campus, Universiti Sains Malaysia, 14300 Nibong Tebal, Penang, Malaysia.*

[2] *Department of Civil Engineering, Universiti Kebangsaan Malaysia, Bangi 43600, Malaysia.*

[3] *Department of Design, College of Fine Arts, Al-Turath University, Baghdad, Iraq.*

[4] *Energy Research Unit, Al-Hawija Technical Institute, Northern Technical University, Kirkuk 36001, Iraq.*

Received 16 July 2024; Revised 22 November 2024; Accepted 26 November 2024; Published 01 December 2024

Abstract

This study investigated the flexural performance of a composite floor system utilizing a profile steel sheet dry board (PSSDB) that was enhanced by adding an additional layer of profile steel sheet (PSS) and infilled with both normal and recycled concrete materials. This improved system is referred to as the double-profile steel sheet dry board (DPSSDB) system. The new DPSSDB concept was proposed to reduce fabrication costs, overall weight, and the depth of the composite floor system compared to traditional composite beam-slab systems. To assess the impact of the additional PSS layer, ten full-scale specimens of both PSSDB and DPSSDB were subjected to four-point static load tests. Additionally, the study investigated the use of lightweight recycled aggregates such as crumb rubber and expanded polystyrene as partial replacements for the aggregates in the infill concrete. The results demonstrated that the DPSSDB system exhibited a 112–170% increase in bending capacity compared to the PSSDB specimens. Partial replacement of concrete aggregates with lightweight recycled materials up to 50% had only a marginal effect on the bending behavior of both PSSDB and DPSSDB specimens compared to those filled with normal concrete. However, replacing 75% of the aggregate with recycled materials led to a 27% reduction in the flexural bending capacity of the DPSSDB specimens compared to those infilled with normal concrete. Additionally, a new method (theoretical equation) was developed to predict the ultimate moment strength (flexural) of the novel DPSSDB composite slab system, which aligned well with the experimental results, achieving a deviation percentage of 0.81% and a mean value of 0.965a.

Keywords: Composite Slab System; Flexural Strength; PSSDB Slab; DPSSDB Slab; Recycled Concrete.

1. Introduction

The development and advancement of composite structural elements focus on achieving greater cost-effectiveness, load-bearing efficiency, reduced weight, environmental sustainability, and ease of construction compared to conventional structures. Among these advancements, the profile steel sheet dry board (PSSDB) system is a lightweight composite floor system consisting of a dry board (DB) and a profile steel sheet (PSS), joined using mechanical self-tapping screws. Wright et al. first proposed the PSSDB floor system in 1989 [1]. Subsequently, in 2002, Ahmed et al. conducted experimental and finite element analyses on two models (isotropic and orthotropic) of two-way slabs and found that the isotropic model was more accurate for practical design purposes, though the orthotropic model was also acceptable [2]. Various aspects of composite PSSDB slabs (DB, PSS, connectors, and infill materials) have been investigated in different studies.

* Corresponding author: cefatimah@usm.my

http://dx.doi.org/10.28991/CEJ-2024-010-12-03

Several researchers have studied the effects of DB. Three studies conducted experiments and finite element analyses on multiple types of DB (plywood, cement board, and chipboard) with different thicknesses, demonstrating that DB has great potential as a component in load-bearing structural systems [3–5]. Other studies have examined the effects of dynamic loading on these types of DB, demonstrating that they provide satisfactory vibration performance for building occupants [6]. The effect of the second component (PSS) on the slab behavior was first investigated by Wan et al., who studied the performance of PSSDB under fire conditions. They compared various types of PSS (Buildeck and Peva45) and different types of DB (tiles and normal concrete) filled with either polystyrene blocks or cement mortar. The results indicated that the PSSDB system exhibited good fire resistance performance [7]. Subsequent studies showed that PSS significantly increases bending capacity, with improvements of up to 18% [8–10].

Research on the third component (connectors) of the PSSDB slab indicated a minor effect on the bending capacity but improved the stiffness, as shown in numerous studies [3, 11]. The behavior of the connections was also studied under dynamic and human walking loads, revealing that reducing screw spacing can decrease the dynamic response, leading to improved comfort levels during use [12, 13].

Various numerical and experimental studies have investigated the fourth component (infill materials) of the PSSDB slab system's structural performance when filled with different concrete materials (normal and foam) [8, 9, 14] and found that the core concrete material in this slab system slightly enhanced the performance and bending strength compared to the same system without an infill material, and it helped to prevent or delay local buckling in the PSS component. Jaffer et al. examined the effects of loading a PSSDB one-way slab system filled with normal and geopolymer concrete materials and found higher rigidity (approximately 43%) and a higher ultimate load (approximately 12%) for geopolymer infill than for normal infill [15–17]. Subsequent studies explored various factors under different load scenarios for infilled specimens, such as developing compressive membrane action [18, 19], the effects of impact loads, vibration response, natural frequency, comfort level [20, 21], heel-drop testing [22], and dynamic behavior under an explosion load [23]. This overview confirms that the PSS has a greater impact on PSSDB behavior than the other components, which is a critical consideration for the current research.

However, despite being filled with concrete, the thin cross-section of the composite floor PSSDB is considered a slender element, causing failure with high deflection, making it suitable only for limited span lengths. Therefore, when filled with concrete materials, the PSSDB composite slab system requires a connection or combination with a steel I-beam, as illustrated in Figure 1(a); this is known as a conventional steel I-beam composite slab system [24]. Nevertheless, because the PSSDB deck slab is filled with concrete and has a thin cross-section, problems arise when shear studs are required to connect the upper flange of the I-beam steel. To support this type of PSSDB-filled concrete composite floor, a different beam or alternative connection method is necessary to achieve longer spans and higher moment capacities.

Over the last twenty years, many researchers have studied the bending moment performance of newly system of composite concrete-filled steel tube (CFST) beams. The CFST composite beam offers many advantages, including cost-effectiveness, ductility, and high strength, compared with other types of composite steel-beam-concrete systems [25, 26]. These investigations used various analytical approaches (numerical and experimental) and different loading conditions (static, impact, and cyclic) [27–29]. Additionally, the use of cold-formed steel tube sections in CFST beam systems has been proposed, because these can be formed with different thicknesses and shapes according to the design requirements [30–32]. Therefore, the CFST beam connected to the PSSDB slab forms a hybrid beam-slab system called CBPDS, filled with normal and recycled concrete [33, 34], to improve the load-bearing capacity of the slab and allow for longer spans, as shown in Figure 1(b). However, the CBPDS system still has disadvantages, including heavier weight, greater depth, and more complex preparation compared to the PSSDB slab system, owing to the CFST beam component. Hence, the first aim of this research is to investigate the effect of using a portion of PSS as an additional lower layer in the PSSDB composite floor system to create a new floor system, the double-profile steel sheet dry board (DPSSDB). This new DPSSDB composite slab is proposed as an alternative to the steel beam concrete slab system and/or the CBPDS slab system, aiming to achieve a thinner depth, lighter weight, easier on-site preparation, and moderate span length.

The current trend is to develop sustainable alternatives to traditional materials. Several researchers have used different types of lightweight recycled aggregates to replace fine and coarse aggregates in infill concrete materials with composite structural elements. These waste materials primarily include crumb rubber aggregates (CRA) [35–37] and expanded polystyrene (EPS) granules as partial replacements for coarse aggregates, which are considered successful methods for creating lightweight recycled concrete mixtures [38, 39]. Recent studies on the mechanical properties of these materials have shown that they are effective in reducing the cost and weight of concrete mixtures [40, 41]. To date, only Al-Shaikhli et al. have investigated the impact of using recycled EPS as a lightweight concrete mixture in two-way PSSDB slabs [8]. Liejy et al. examined the effects of four types of recycled materials (crumb rubber, EPS, crushed concrete, and fine glass) in concrete mixtures on the bending strength of a CBPDS [33]. Therefore, further investigation of the newly proposed DPSSDB composite slab is required, particularly regarding the use of recycled materials. Therefore, the second aim of this study is to examine the bending behavior of a new DPSSDB specimen filled with recycled concrete waste containing high proportions of lightweight recycled aggregates. This approach aims to reduce overall cost, weight, and environmental impact. The third aim was to develop a new analytical method (theoretical equation) using a stress block diagram to calculate the nominal bending moment (flexural) of the newly proposed DPSSDB composite slab system.

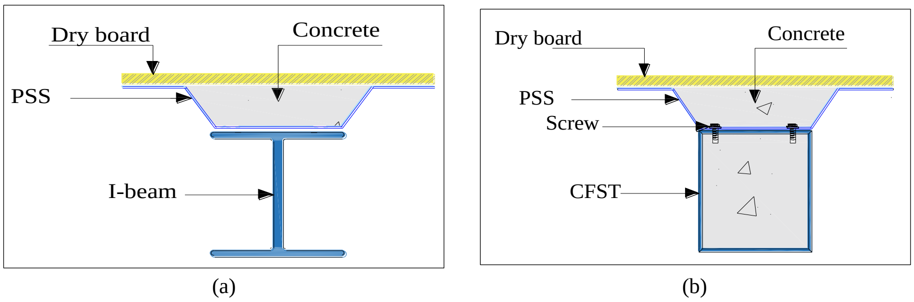

Figure 1. Beam-Slab composite system: (a) I-beam steel-slab; (b) CFST beam-slab

The research began with an experimental investigation. Ten specimens, divided into the PSSDB and DPSSDB categories, were prepared and categorized as follows: i) one unfilled specimen, ii) two specimens filled with normal concrete, iii) one specimen partially filled with normal concrete, and iv) six specimens filled with recycled concrete using three combinations of lightweight recycled aggregates (fine crumb rubber, coarse crumb rubber, and coarse EPS). These aggregates were used to partially replace 25%, 50%, and 75% of the volume of fine and coarse aggregates. All the specimens were tested under four-point loading. In addition, a new analytical method (theoretical equation) is developed to calculate the nominal moment (M_n) of the proposed DPSSDB composite slab system. Figure 2 illustrates a flowchart of the research methodology.

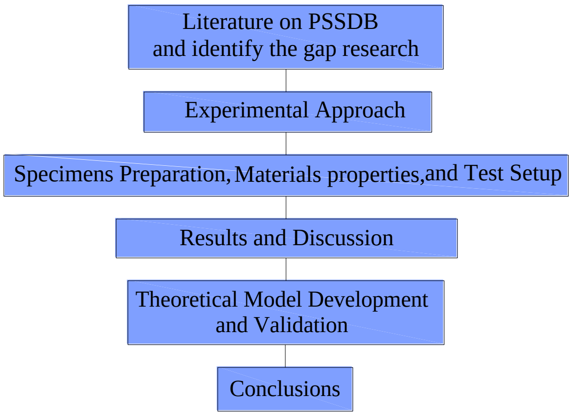

Figure 2. Research flowchart

2. Experimental Approach

2.1. Preparation of Specimens

In this study, ten full-scale, simply supported, composite lightweight slab specimens were prepared and divided into two groups. The first group consisted of PSSDB slabs, which included hollow specimens, specimens filled with normal concrete (control), and specimens filled with recycled concrete comprising 25%, 50%, and 75% lightweight recycled aggregates. The designation ID of the specimen is shown in Figure 3, and the details are presented in Table 1. These specimens were fabricated using profile steel sheets (PSS; 0.8 mm thick, 50 mm deep sections, and 1000 mm wide sections), known as Peva50 in Malaysian markets, and connected with 12 mm cement sheet dry board (DB) (type Prima*flex*) using self-tapping screws (DS 640 HW) for easy and straightforward assembly.

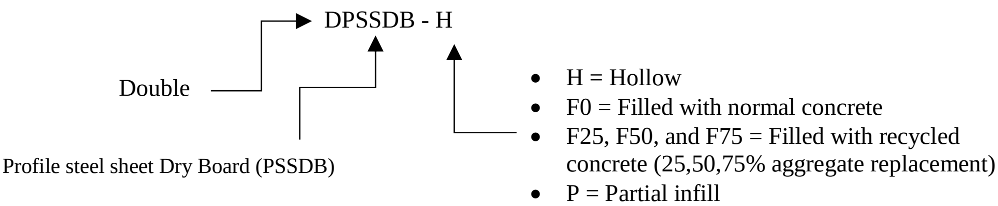

Figure 3. Specimen's designation ID

Table 1. Results and Designations of experiment specimens

Specimens Designation	Infill Concrete	P_u (kN)	M_u (kNm)	MIP (+%)	EAI (kN.mm)	EAI improvement (%)	*ØMn* (kNm)	*ØMn/Mu*
PSSDB-H	Hollow	17.8	6.2	-	396	-	-	-
PSSDB-F0	Fill	20.3	7.1	0	544	0	-	-
PSSDB-F25	Fill	20	7.0	-	520	-	-	-
PSSDB-F50	Fill	20	6.9	-	489	-	-	-
PSSDB-F75	Fill	19.4	6.85	-	480	-	-	-
DPSSDB-F0	Fill	54.8	19.2	170	1342	146	16.71	0.87
DPSSDB-P	Partial fill	45	15.8	122	1084	99	16.31	1.03
DPSSDB-F25	Fill	51.5	18.0	146	1026	88	16.5	0.91
DPSSDB-F50	Fill	49.0	17.2	145	1173	115	16.24	0.94
DPSSDB-F75	Fill	43.2	15.1	112	1041	91	16.07	1.06
Mean Value								**0.965**
Standard Deviation								**0.081**

The second group of specimens consisted of DPSSDB slabs, which were similar to the first group in terms of the type of filling, except that a partial normal concrete filling was used instead of hollow sections. This modification was proposed to strengthen the lower layer of the PSS against damage and shear failure at the support points. All DPSSDB sections were fabricated by connecting an additional PSS layer (two ribs only) to the PSSDB using the same self-tapping screws with a spacing of 195 mm to connect all the elements (PSS with DB and between PSS and the lower additional PSS layer) to prevent shear failure in the screws and facilitate easy preparation. Details of the PSSDB and DPSSDB specimens are shown in Figures 4 and 5, respectively.

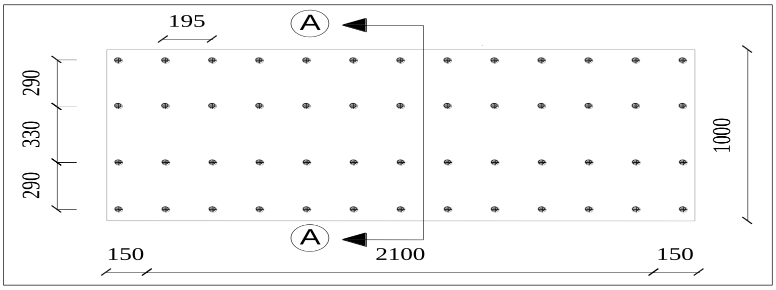

(a)

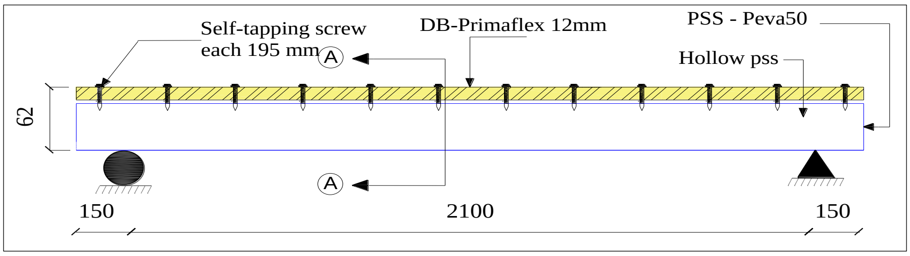

(b)

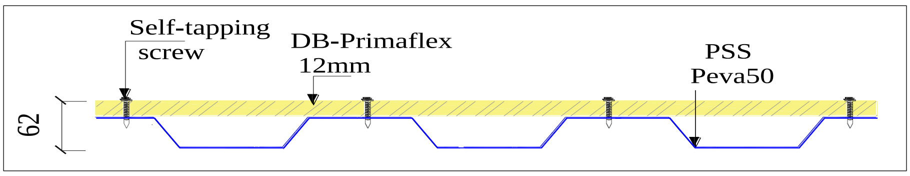

(c)

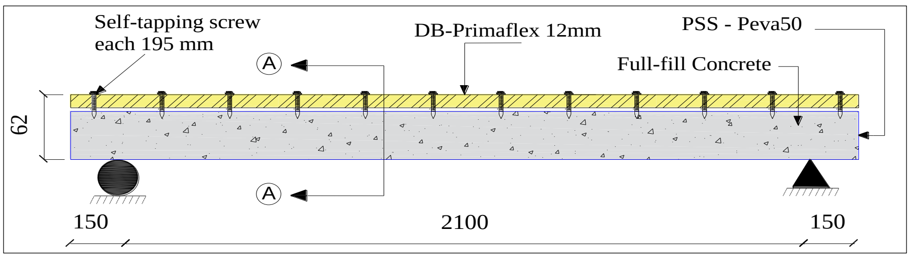

(d)

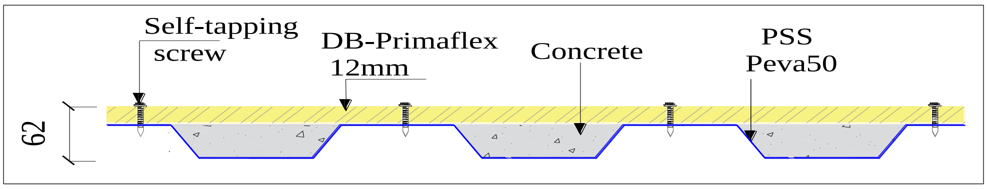

(e)

Figure 4. The composite PSSDB slab system. (a) top view; (b, c) the hollow PSSDB slab system and cross-sectional; (d, e) the infill PSSDB specimen details and cross-sectional. (All units in mm)

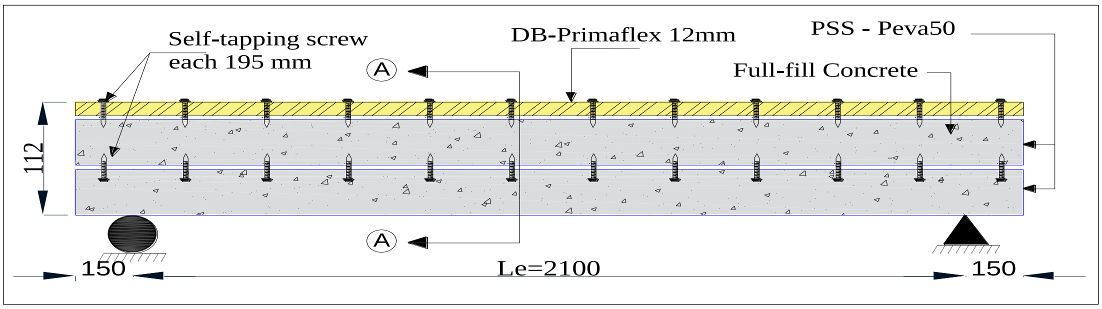

(a)

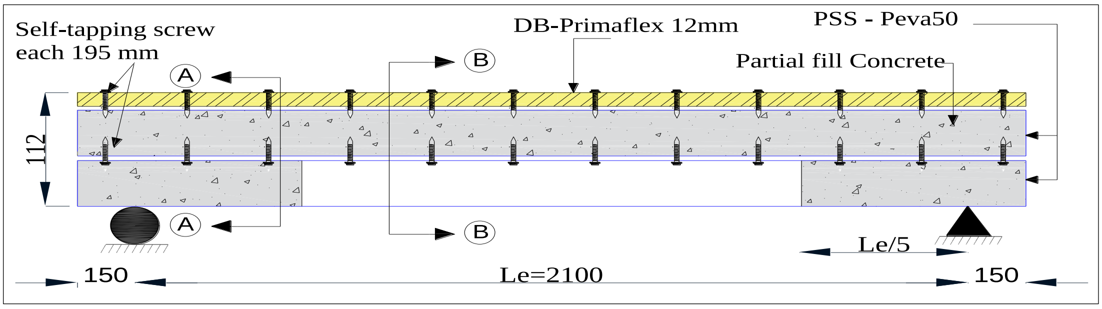

(b)

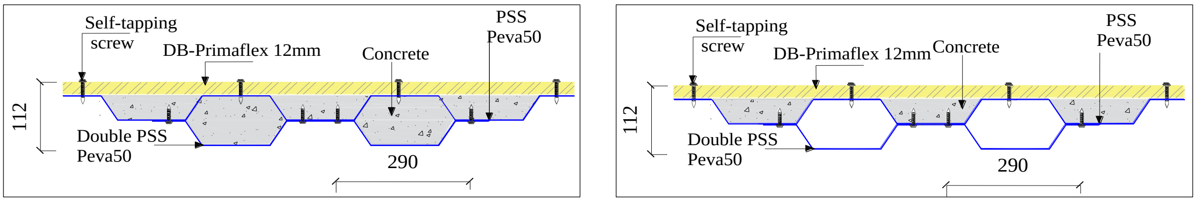

(c)

Figure 5. The composite DPSSDB slab (all dimensions in mm). (a) Elements of DPSSDB-F0 specimen; (b) Components of DPSSDB-P specimen; (c) Cross sections for DPSSDB. (All units in mm)

The process of pouring concrete into the DPSSDB slabs was more challenging because of their two-layer structure. To pour concrete across the surface and inside the ribs of the PSS, a new technology was required to facilitate the process, particularly when the DPSSDB specimen was positioned horizontally (as in typical site conditions). To achieve this, several circular openings (50 mm in diameter at 350 mm c/c) were drilled successively into the PSS side web. The locations of these openings were carefully selected to avoid interference with the areas of the point load, maximum shear, and maximum moment deflection. These circular perforations are simple and easy to create on-site using an electric drill, as illustrated in Figures 6-a and 6-b. For the specimens with partial infill concrete (DPSSDB-P), a small partition of DB was positioned at one-fifth of its length from the support point and secured in place with epoxy, as shown in Figure 6-c.

All components of the PSSDB and DPSSDB were connected using self-tapping screws 40 mm long and 6 mm in diameter. The confined concrete inside the PSS groove was secured by the additional length of the screws acting as embedded connectors, a scenario similar to that confirmed in previous studies [34, 42]. Portions of the dry board were used to temporarily seal the open sides of the PSS during concrete casting for 24 h. An electric vibrator was employed in the time of pouring to eliminate air pockets in the concrete. Finally, once the concrete hardened, the DB was placed on the PSS and connected using screws, as shown in Figures 6-d and 6-e.

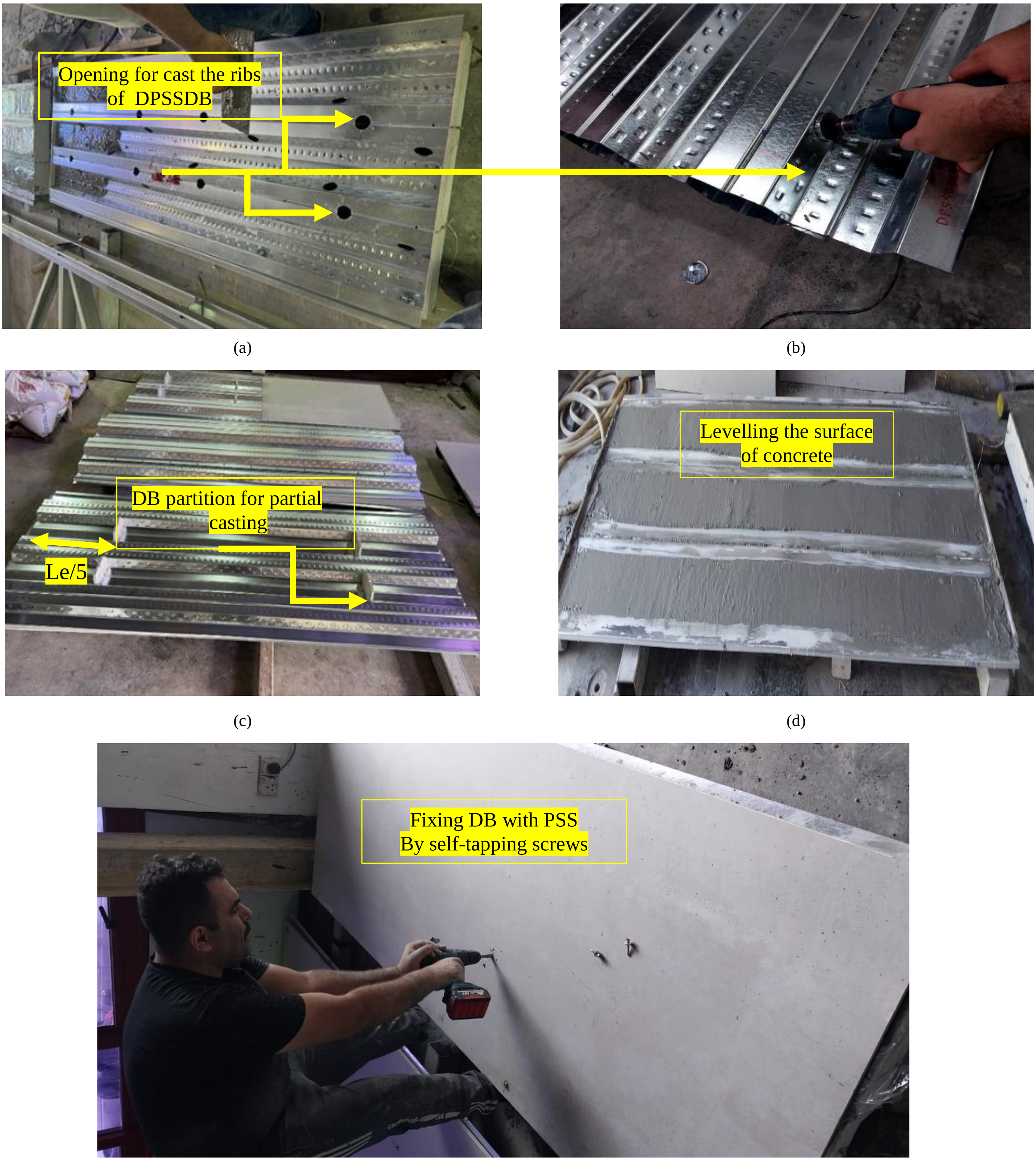

(a) (b) (c) (d) (e)

Figure 6. The Preparation stages composite slab system. (a, b) Opening by drill to cast the ribs of DPSSDB; (c) DB partition for DPSSDB-P; (d) Levelling the surface of concrete; (e)connected DB with PSS for all specimens

2.2. Material Properties

The Peva 50 was employed as profile steel sheet (PSS) to create the DPSSDB floor system because of its substantial rib width and characteristics, which are suitable for infill concrete material [17, 43]. The physical properties of PSS were determined through direct tensile testing of three samples prepared in accordance with the ASTM-E8M/8M-09 standards [44]. The composite method employed a cement board (DB) known as Prima*fl*ex, which is the same DB sheet used in previous studies [8, 45]. Table 2 illustrates the properties of both the PSS and the DB. Self-tapping self-screws (DS 640 HW) were selected to link the components of the proposed DPSSDB composite floor.

Table 2. Properties of materials

Materials	Elastic modulus (GPa)	Yield strength (MPa)	Ultimate strength (MPa)
PSS (Peva 50)	213	434	464
DB (Prima*flex*)	8.03	-	22

Four concrete mixtures were prepared and used as filling material for the PSSDB and DPSSDB specimens, each comprising a several quantity of lightweight recycled aggregates: 0% (F0), 25% (F25), 50% (F50), and 75% (F75). These lightweight recycled aggregates included crumb rubber, manufactured in Malaysia by Yong Fong Rubber Industries Sdn Bhd, distributed into two sizes (CRCA and CRFA), and EPS, which partially replaced the fine and coarse aggregates by volume. The concrete mixture consisted of 460 kg/m³ of ordinary cement (CASTLE, made in Malaysia), fine sand (density of 1460 kg/m³), and 20 mm diameter crushed coarse aggregate (density of 1502 kg/m³).

The concrete samples were prepared and cured according to the BS1881-1983 standards. To enhance the compressive strength and workability of the concrete mixture for easy pouring into the DPSSDB specimens, a high water/cement ratio of 0.5, along with a superplasticizer (4 ml/kg of cement weight, Fosroc Sdn. Bhd. CONPLAST AP) and Elkem Microsilica 920, which replaced 10% of the cement weight. This study utilized a combination of three lightweight waste materials as recycled aggregates (EPS, CRCA, and CRFA), as illustrated in Figure 7. The densities of the lightweight recycled aggregates were 9.5 kg/m³, 595 kg/m³, and 686 kg/m³ for EPS, CRCA, and CRFA, respectively. From each mixture, three cubes (150 mm) were taken and tested 28 d later in accordance with BS1881-Part 116 [46]. Table 3 lists the mixture proportions and results for the tested concrete samples.

EPS (6.3 mm) CRCA (4-8 mm) CRFA (1-4 mm)

Figure 7. Three types of applied lightweight recycled aggregates

Table 3. Concrete mixtures proportion (per 1 m^3) and results of the tested concrete samples

Mixture ID	Cement (kg)	Fine Agg. (kg)	Coarse Agg. (kg)	Water (L)	EPS (%)	CRCA (%)	CRFA (%)	Density (kg/m^3)	f_{cu} (MPa)	Reduced f_{cu} (-%)	E_c (GPa)
F0	460	585	1090	230	0	0	0	2346	27.9	-	24.8
F25	414	527	927	230	5	10	10	2175	22.1	20.7	22
F50	414	468	763	230	10	20	20	2039	14.7	47.3	18
F75	414	410	600	230	15	30	30	1907	10.1	63.7	14.9

2.3. Test Setup

All PSSDB and DPSSDB specimens were tested under a four-point bending static load (simply supported span), as illustrated in the schematic of the test setup in Figure 8. The load was applied using a hydraulic jack and distributed equally across the specimen using a two-line load. This study applied a two-point load to achieve a half-sine wave, which is a nearly uniform load; this technique is related to previous studies [9, 34]. Three linear variable displacement transducers (LVDTs) (KYOWA, Osaka, Japan) were positioned below the specimen to calculate the vertical deflection at three different places: the center point plus two points at quarter length Le/4 from the support of the specimen. Additionally, four strain gauges (SG) were employed for the PSSDB specimens and five for the DPSSDB specimens. The strain gauges (KFGS-30-120-C1-11 L5M2R, manufactured by KYOWA, Japan) were placed horizontally at the middle length of the section and numbered as follows: SG1 was fixed on the upper of the DB center (maximum compressive region), SG2 on the top flange of the upper PSS section, SG3 on the web of the upper PSS (at the link level with the PSS slab), SG4 on the bottom flange of the upper PSS section, and SG5 (used only for the DPSSDB) on the bottom flange of the lower PSS (maximum tensile region). For further clarification, see Figures 8 and 9.

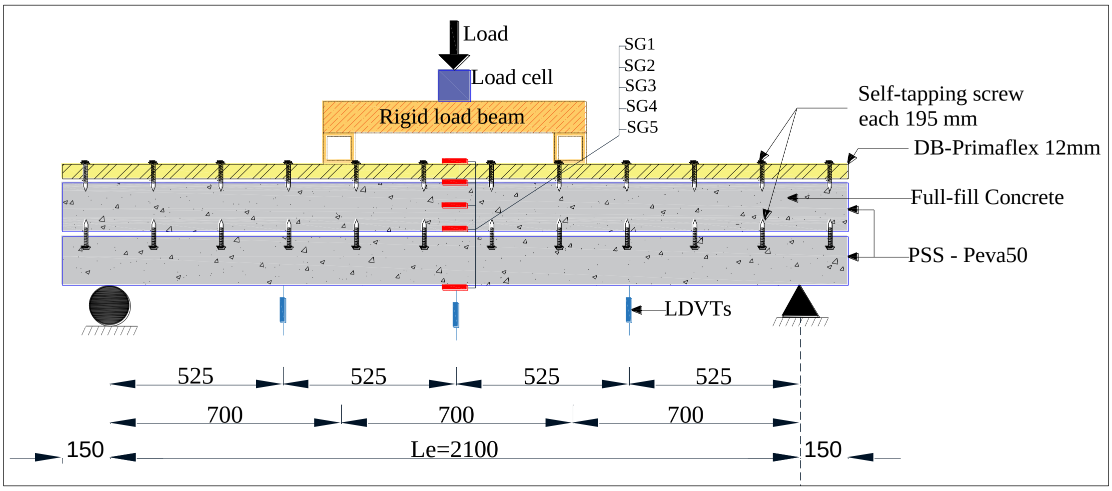

(a)

(b)

Figure 8. The test setup of the DPSSDB specimen; (a) Schematic test setup; (b) actual test setup (all unit in mm)

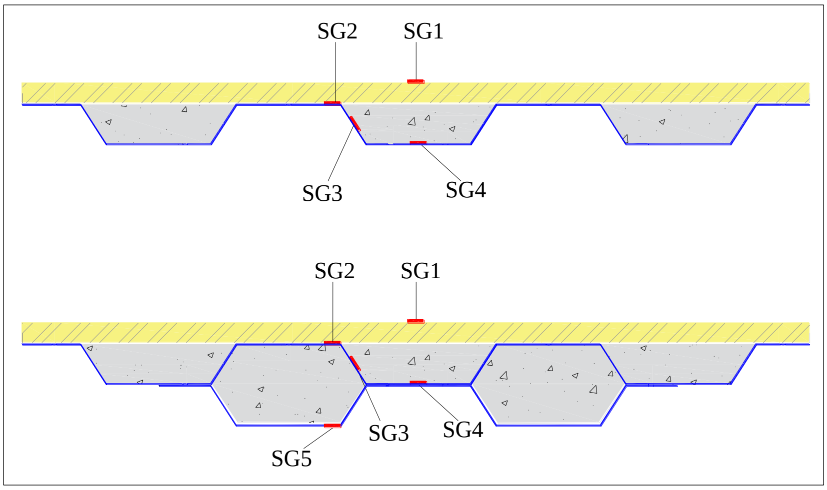

Figure 9. The strain gauges distribution in the PSSDB and the DPSSDB specimen

A hydraulic jack was used to apply the incremental static point load at a rate of 0.07–0.12 kN/sec above the center of the sample, which was distributed by two hollow square steel beams to create two line loads as designed in the boundary condition. A load cell transmits the reading values through a data logger set between the actuator and load beam. The measurements obtained from the strain gauges, LVDTs, and load cell were recorded and saved on a laptop using Microsoft Excel.

3. Experimental Results and Discussions

3.1. Failure Modes

The PSSDB and DPSSDB specimens exhibited typical and similar bending behaviors. The region between the two load points, specifically the dry board (DB) and the top flange of the upper PSS, experienced compressive stress, whereas the bottom flange of the PSS below the neutral axis (NA.) was subjected to tensile stress. This behavior is consistent with the performance observed in composite beam-slab systems tested by Liejy et al. [33, 34]. The tests on the specimens extended beyond their bending limits, resulting in significant compressive stress, which led to local buckling failure at the top flange and web of the PSS, as shown in Figure 10.

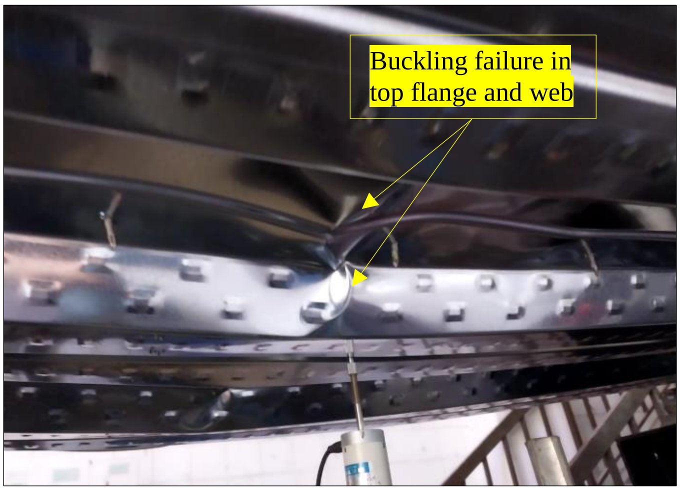

Figure 10. local buckling behavior of the PSSDB specimens

Among the PSSDB specimens, the hollow PSS specimen (PSSDB-H) exhibited twisting failure and outward local buckling of the PSS's cross-section (flange and inclined web) early in the loading phase (50-60%), as depicted in Figure 11. The PSS ribs were too thin to sustain the compressive force transmitted directly from the load. As the load reached 70-80% for PSSDB-F0, PSSDB-F25, PSSDB-F50, and 60-70% for PSSDB-F75 of the specimen's ultimate bending capacity, similar outward local buckling was observed at the upper flange of the PSS section, which then spread throughout the entire PSS section, attributed to the presence of infill material. Additionally, DB cracks under the loading lines, twisted screws toward the center of the slab, and slip failure in the concrete core were observed after the load exceeded 90% of the ultimate capacity, as illustrated in Figure 12.

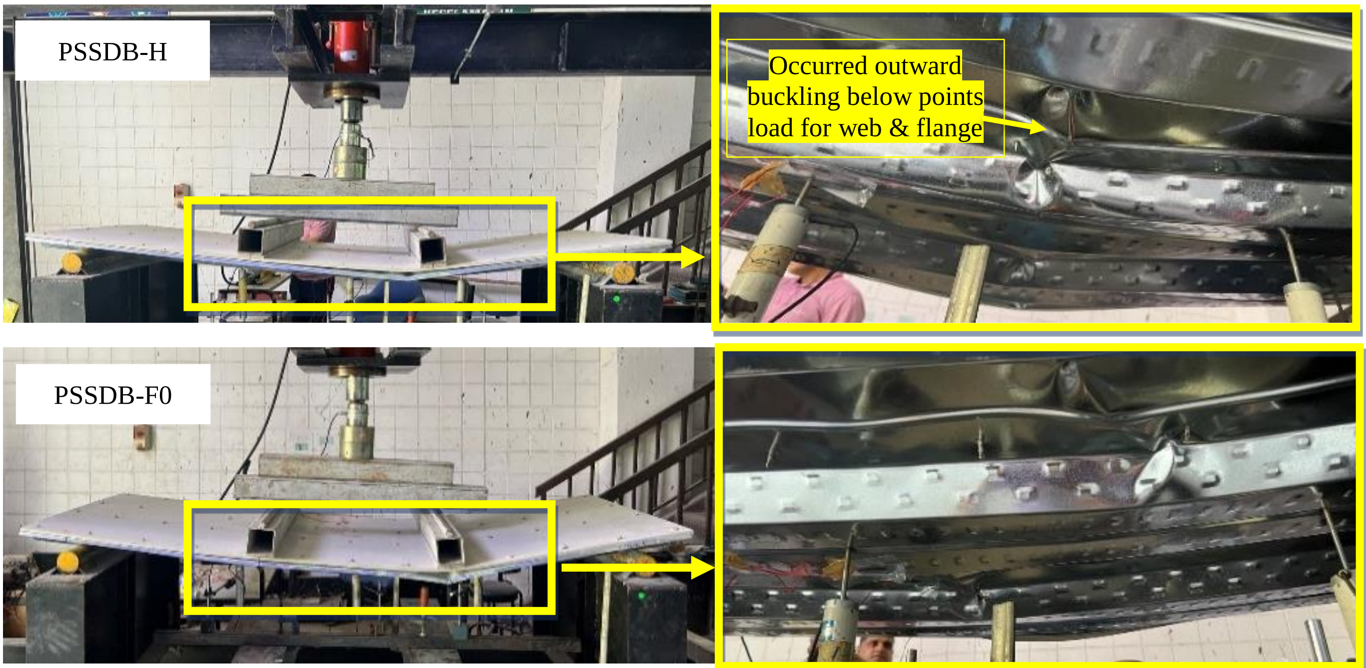

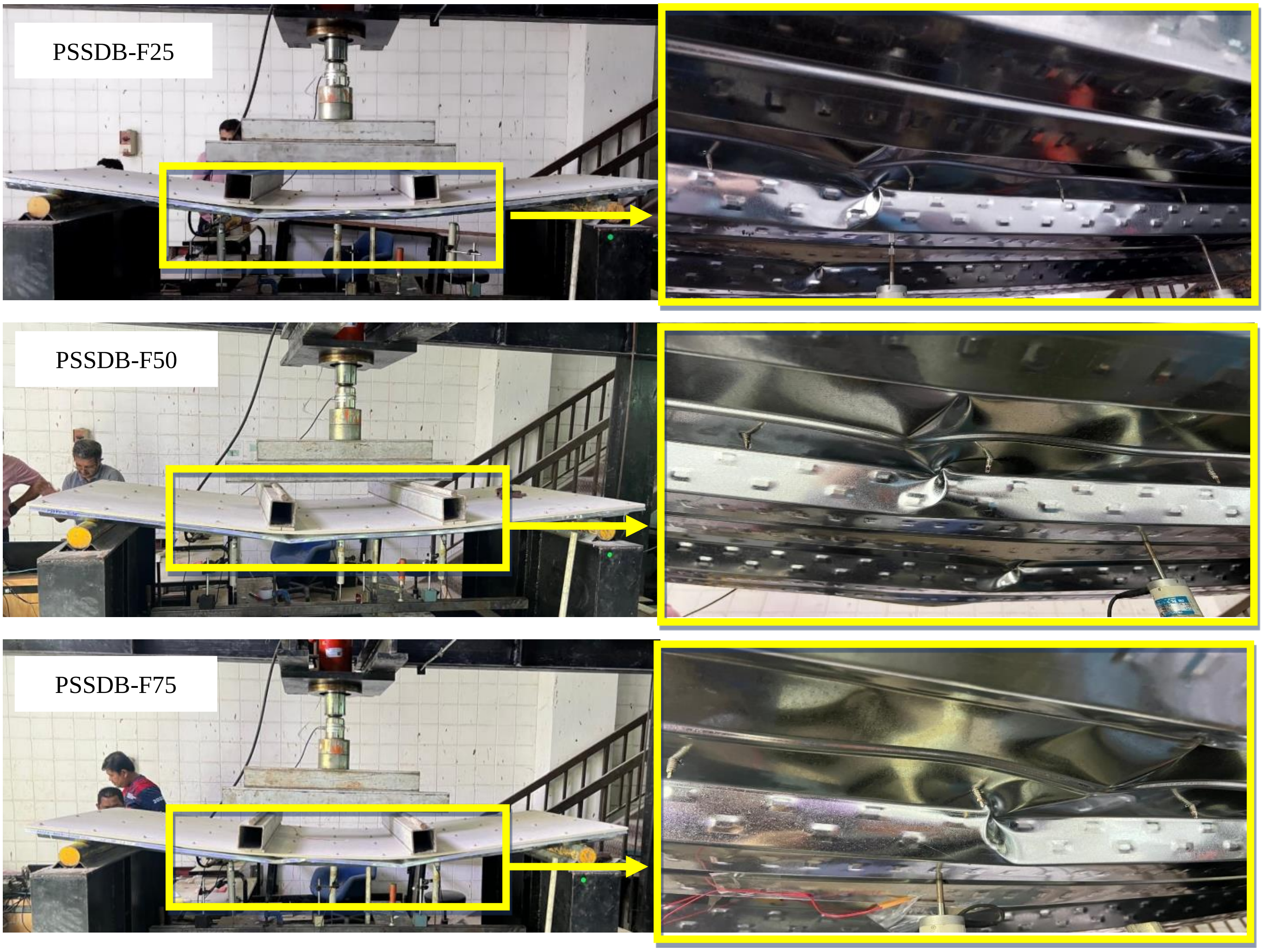

Figure 11. Bending behavior of the PSSDB hollow and filled concrete specimens

Figure 12. Observed various failures of the PSSDB specimens

However, the new DPSSDB specimens (filled with normal and lightweight recycled concrete) exhibited better resistance to local buckling failure than the corresponding PSSDB specimens, as shown in Figure 13. Buckling failure in the DPSSDB specimens began at about 80-90% of their ultimate capacities. For the DPSSDB-P specimen (with partial infill concrete), debonding occurred between the DB and PSS in the side wing at approximately 90% of the loading capacity because of the hollow space in the partial filling type, as illustrated in Figure 14. Additionally, the upper-core concrete displayed longitudinal splitting owing to the lack of support at the ends of the sample, as shown in Figure 14. Longitudinal cracks in the DB occurred in the DPSSDB-F75 between the line load and support when it reached 90% of its ultimate load capacity, as shown in Figure 15. The infill concrete materials in the lower PSS ribs of the DPSSDB specimens significantly affected the slab system, even with higher percentages of recycled aggregates (25%, 50%, and 75%), without significant differences in failure mode compared with the corresponding sample filled with normal concrete (0% recycled aggregates). Moreover, there was no slip failure in the concrete core for any of the DPSSDB specimens because of the excellent bond between the steel and concrete, facilitated by the holes made for pouring the concrete and the embedded length of the self-tapping screws used to connect the additional PSS to the PSSDB slab.

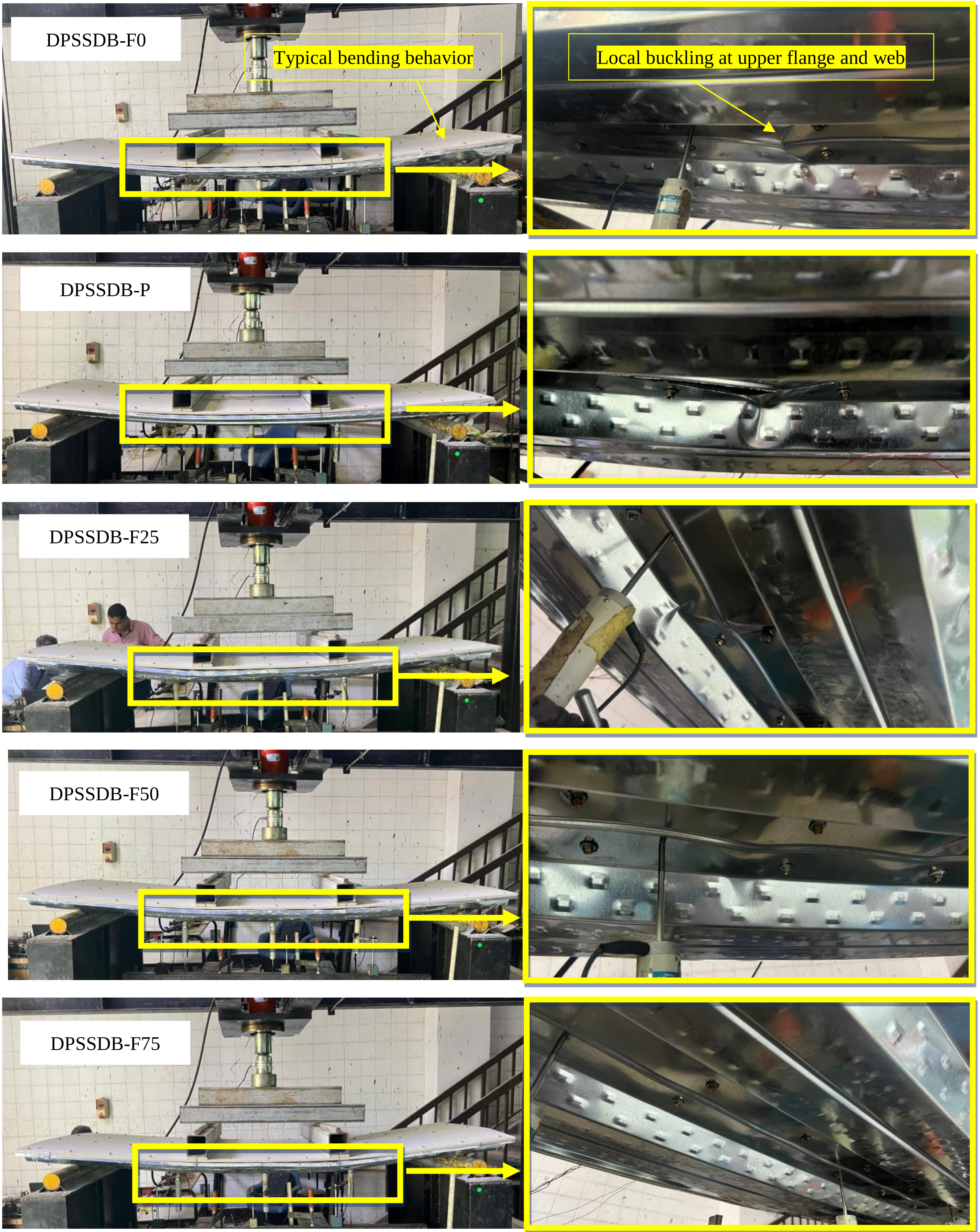

Figure 13. Bending behavior of the PSSDB hollow and filled concrete specimens

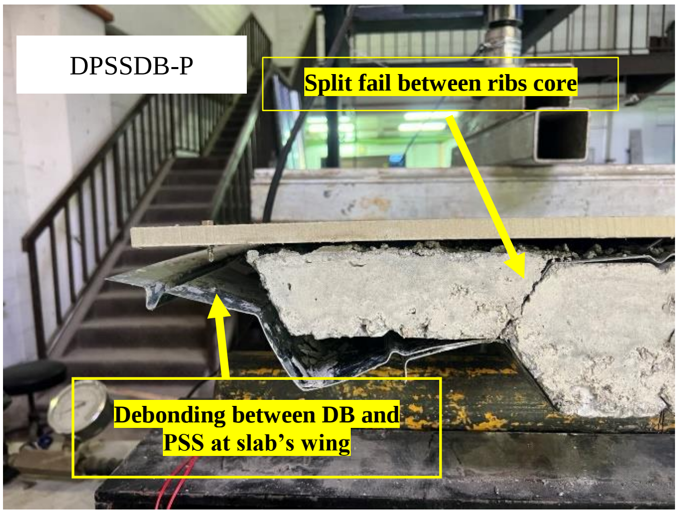

Figure 14. Debonding failure of DPSSDB-P specimens

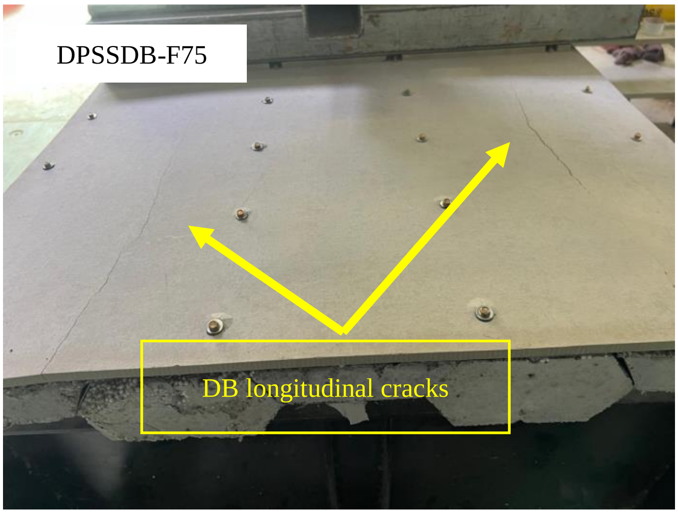

Figure 15. DB crack pattern of DPSSDB-F75 specimens

Furthermore, no crushing failures were observed in the DB sheet or filling concrete core within the PSSDB floor, and no shear failures occurred in the screws until the end of the test, confirming the excellent bonding between the specimen components (DB-PSS and PSS-PSS ribs). The efficiency was maintained until the applied load reached the ultimate bending moment of the specimen. However, the circumference of the opening was slightly twisted and buckled when the load reached about 85% of the specimen's capacity. This indicates that these openings and their estimated locations did not lead to significant weakness slab's bending behavior.

Based on the relationship between the deflection at the three points obtained by the LVDTs and the moment capacity at the four limits (0.25 *Mu*, 0.5 *Mu*, 0.75 *Mu*, and 1 *Mu*), all samples (PSSDB and DPSSDB) exhibited deflection behavior that closely resembled a half-sine curve (Figure 16).

3.2. Moment vs. Deflection Relationships

Figure 17 compares the moment versus deflection relationships for different types of specimens, including control PSSDB slabs (hollow and infilled with normal concrete), PSSDB slabs infilled with recycled concrete, and DPSSDB slabs infilled with both normal and recycled concrete. The PSSDB-H and PSSDB-F0 specimens exhibited similar elastic-plastic behavior up to failure, with moments of 6.2 and 6.7 kN.m, respectively, measured at maximum deflections equal to Le/50, as shown in Figure 17-a. The slope of the curve continuously decreases as the PSS begins to buckle under point loads and then sharply declines after this stage. The bending moment increased by 8% owing to the efficiency of the infill material and the effective bonding between the PSS, DB, and concrete core surface, which helped delay the onset of local buckling in the PSS.

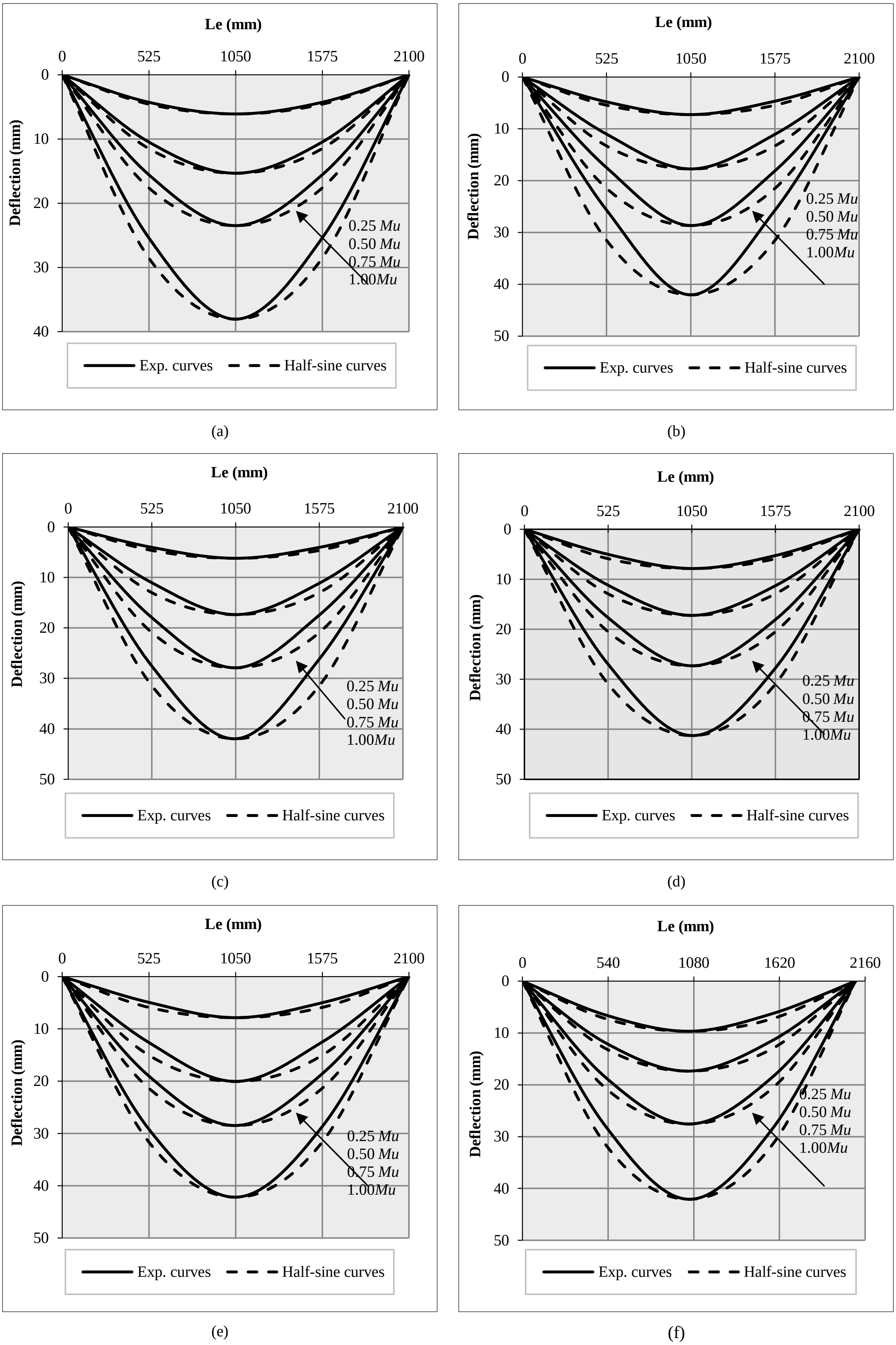

Figure 16. Deflection curves of PSSDB and DPSSDB specimens. (a) PSSDB-H; (b) PSSDB-F0; (c) PSSDB-F25;(d) DPSSDB-F0; (e) DPSSDB-P; and (f) DPSSDB-F25

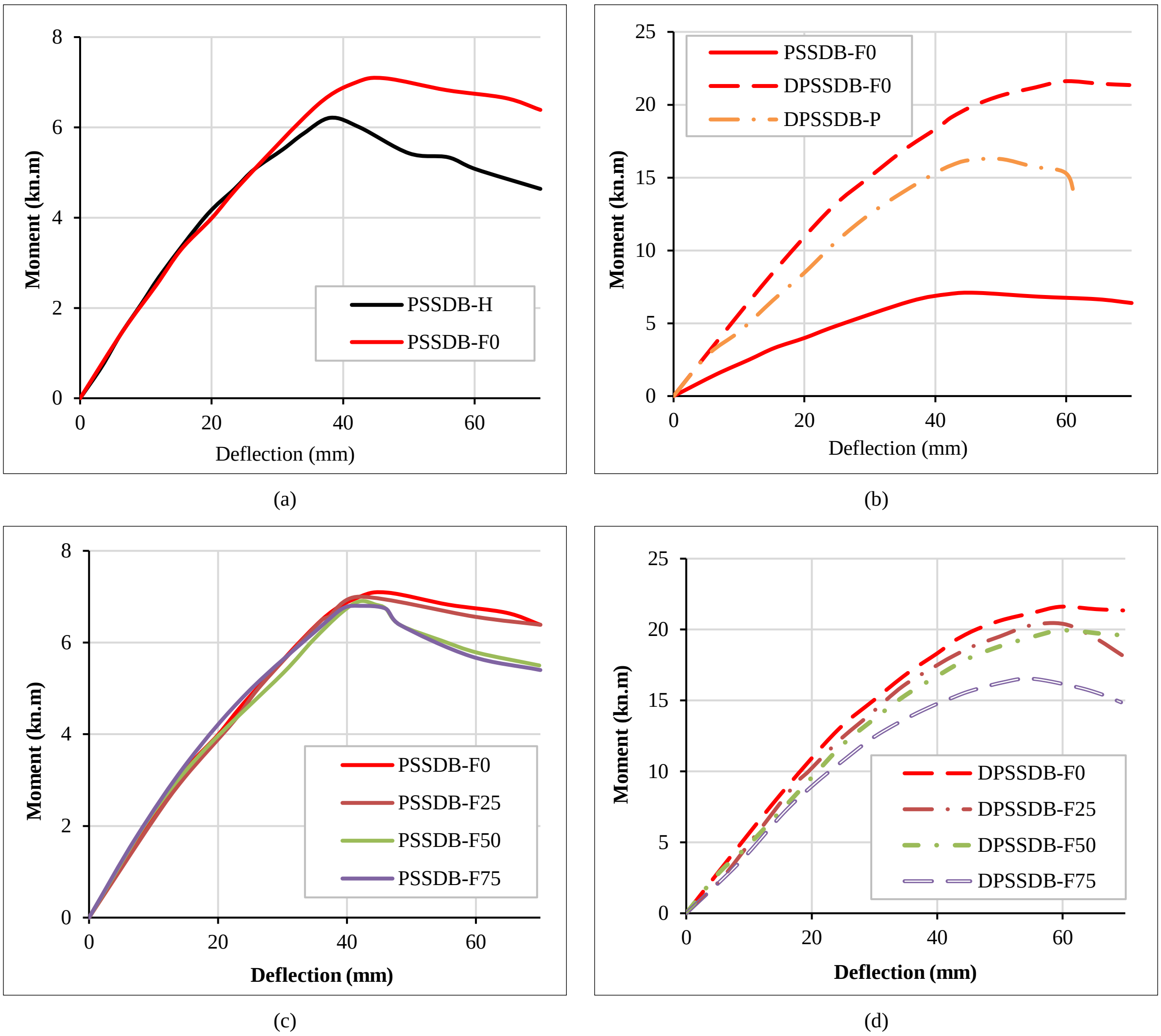

Figure 17. Moment vs mid-span displacement graphs. (a) Comparison PSSDB (hollow and infill with F0); (b) Comparison PSSDB-F0 with DPSSDB (infill partial and F0); (c) PSSDB specimens; (d) DPSSDB specimens

The DPSSDB-F0 and DPSSDB-P specimens demonstrated stiffer flexural behavior in the linear elastic zone, achieving approximately 65% of the maximum bending capacity compared to the PSSDB-F0, as shown in Figure 17-b. The ultimate bending moments reached 19.2 kN.m and 15.8 kN.m, respectively. DPSSDB-F0 continued to display elastic-plastic behavior, achieving a failure bending moment of 21.8 kN.m, while DPSSDB-P's curve began to decline, with a failure bending moment of 16.1 kN.m, as the PSS (flange and web) started to buckle under the point load until the end of the test. This indicates ductility even after exceeding the ultimate bending capacity deflection limits. The high ductility of DPSSDB-F0 and DPSSDB-P can be attributed to the new technique of adding a lower PSS layer (creating double-layer ribs) and confined concrete infill, which prevents or delays PSS buckling failure, as well as the strong bonding between the PSS, DB, and concrete core. Overall, the composite slab specimens DPSSDB-F0 and DPSSDB-P exhibited more rigid flexural performance, with ultimate moments increasing by an impressive 170% and 122%, respectively, compared to the control specimens (PSSDB-F0), as shown in Figure 17.

Specimens with 25%, 50%, and 75% recycled aggregates (PSSDB and DPSSDB) displayed similar behavior curves, however bending performances slightly reduced compared to their corresponding specimens (PSSDB-F0 and DPSSDB-F0), particularly during the plastic loading stage, as shown in Figures 17-c and 17-d. This reduction in the ultimate bending moment can be attributed to the lower compressive strength (f_{cu}) of recycled concrete.

3.3. Moment vs. Tensile Strain Relationship

Figure 18 illustrates the relationship between the moment and strain values for the investigated specimens with the strain gauge placements illustrated in Figure 9. In the control slab (specimen PSSDB-F0), strain gauges SG1-PSSDB and SG2-PSSDB exhibited an upward relationship between compressive values and the bending moment. The SG1-PSSDB was attached to the upper surface of the DB, and the SG2-PSSDB was attached to the top flange of the PSS, both located at the mid-span distance (Le). Meanwhile, SG3-PSSDB and SG4-PSSDB, which were placed on the upper

PSS web and bottom flange, respectively, in the PSSDB-F0 specimen exhibited an upward relationship between tensile values and the bending moment., as illustrated in Figure 18-a. The other PSSDB specimens with different infill types (25%, 50%, and 75% recycled concrete) exhibited similar moment–strain relationships, indicating that the type of recycled concrete material did not significantly affect these relationships.

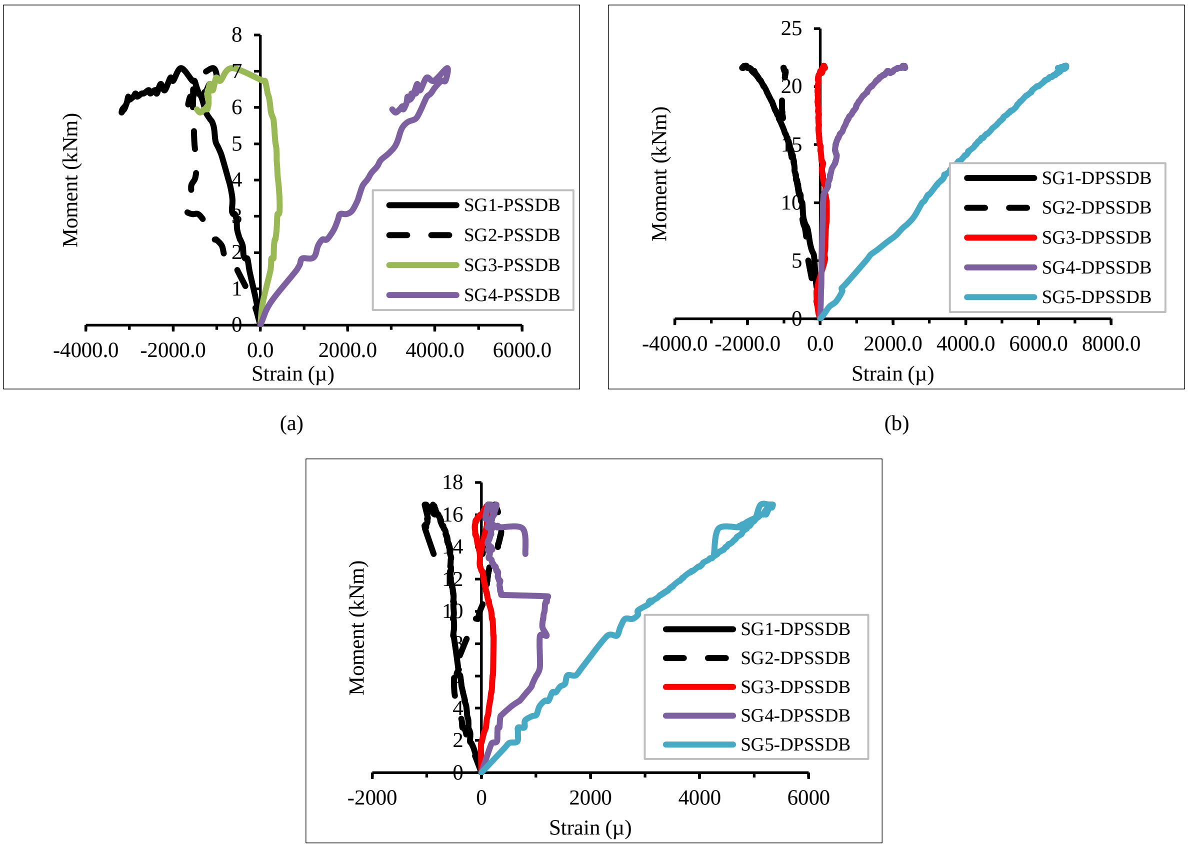

(a) (b)

(c)

Figure 18. The relationship between moment and strain. (a) PSSDB-F0; (b) DPSSDB-F0; (c) DPSSDB-P

Figure 18-b shows the moment–strain relationship for the DPSSDB-F0 slab, which has a double-profile steel sheet filled with normal concrete. SG1-DPSSDB and SG2-DPSSDB consistently recorded increasing compression (negative) strain readings during testing. These gauges were positioned at the mid-span distance (*Le*) on the upper face of the DB and on the PSS's top flange, as shown in Figure 9. The SG3-DPSSDB, fixed on the inclined web of the top PSS, initially recorded slight tension (+positive) strain values until the moment reached 14 kN.m, after which it recorded slight compression (negative) strain values, indicating that the neutral axis for the DPSSDB specimen was located at the transition point (the middle of the upper PSS web). SG4 and SG5, positioned on the upper and lower flanges of the additional PSS rib, respectively, showed a continued increase in tensile strain (positive) readings. Notably, SG1-DPSSDB, SG2-DPSSDB, SG3-DPSSDB, and SG4-DPSSDB did not reach the yield point even at the end of the loading test, whereas SG5-DPSSDB reached the yield limit at 70% of the bending capacity. The specimen with a double-profile steel sheet and partial filling with normal concrete (DPSSDB-P) exhibited a similar moment–strain relationship, as shown in Figure 18-c.

3.4. Bending Moment Capacity

The ultimate bending moment capacity (*Mu*) of the examined composite PSSDB and DPSSDB floors was determined by evaluating the uttermost point of the moment-deflection curve or by selecting the moment value corresponding to a maximum deflection limit equal to *Le/50*, whatever occurred first. The *Mu* values of the examined specimens are presented in Figure 19, and previously Table 1 illustrated the moment improvement percentage (MIP) between the values of the specimens with various infill formations (double filling and double partial filling) and their control specimen (PSSDB-F0). The bending moment capacity of the PSSDB-F0 specimen increased until reached approximately 170% when a double PSS sheet was used to become (DPSSDB-F0), and the same specimen's capacity increased by approximately 122% when partial infill concrete material was used (DPSSDB-P specimen).

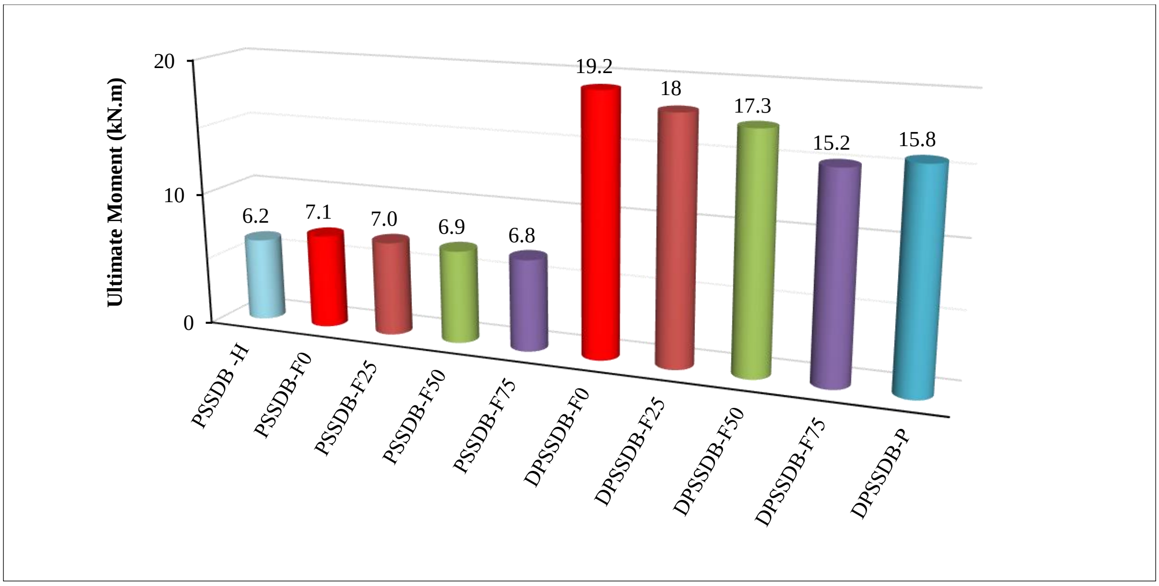

Figure 19. Ultimate moment (*Mu*) capacity for the tested specimens

In general, the improvement obtained in the DPSSDB-F0 and DPSSDB-P specimens was considered economical due to the fact that the additional depth increased to 80%, and self-weight of lower PSS increased to 86% and 42%, respectively, compared with the original self-weight of the corresponding specimen (PSSDB-F0). Compared with the results of Liejy et al. [34], the depth has increased by 223% and the weight has increased by more than 85%, although the moment capacity has increased by 400%. Therefore, the creation of a beam-slab system is considered for a high load and long span, while the composite DPSSDB slab system is considered suitable for a reasonably long span with a thinner depth.

Consequently, the Mu values of the PSSDB and DPSSDB specimens decreased slightly when the percentage of recycled aggregate in the infill concrete material containment increased. As an example, the Mu value of specimen PSSDB-F75 equals 7 kN.m, reduced by 1.5% of the volume aggregate was partially replaced with light recycled aggregates, and the Mu value was reduced by around 21%, from 19.2 kN.m for specimen DPSSDB-F0 to 15.1 kN.m for specimen DPSSDB-F75. Hence, it can be assumed that by using a combination of light recycled aggregates to partially replace 75% of the volume aggregates, the self-weight of the concrete cores in the suggested composite slab specimens was reduced by approximately 13.5-15.4% and resulted in a decrease of approximately 1.5-21% in their Mu values, while having minimal impact on the overall bending behavior.

3.5. Energy Absorption Index (EAI)

The energy absorption index (EAI) of the prepared PSSDB and DPSSDB samples under four-point static loads is explored in this section. The (EAI) of the specimens were measured by determining the cumulative summation of the bar area below the load versus the deflection curve until the upmost point (maximum strength yield limit of the specimen), as shown in Figure 20.

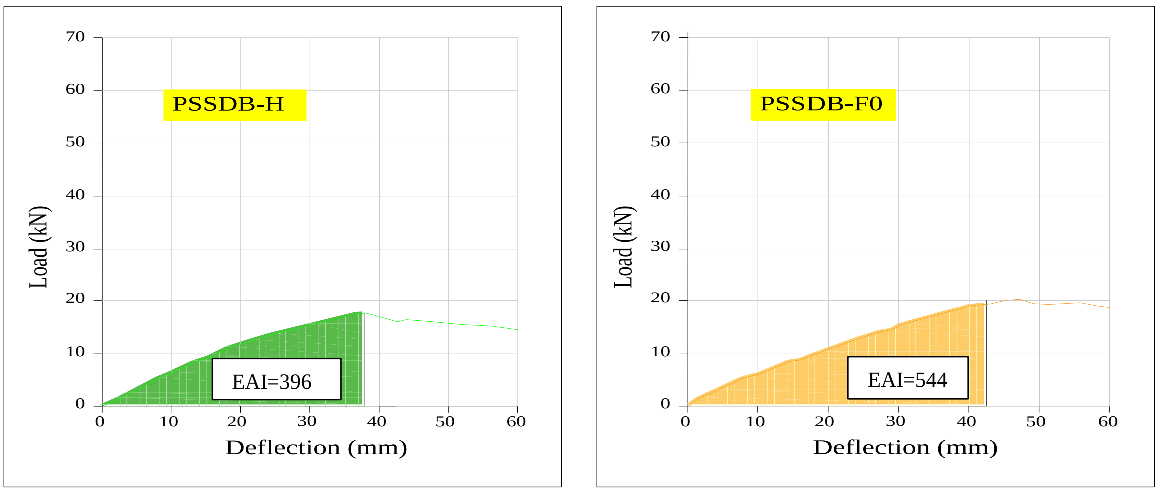

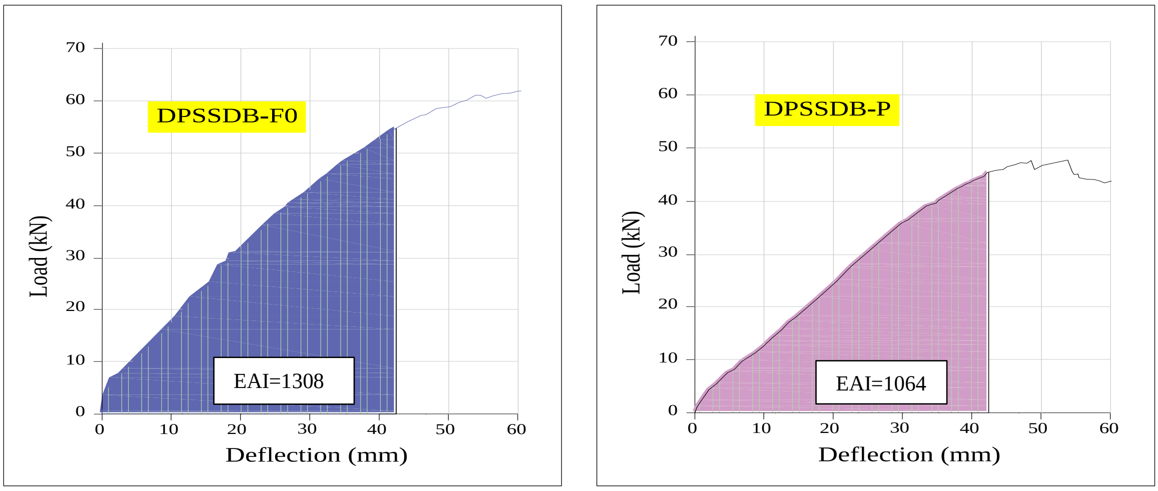

Figure 20. The load-deflection curve for estimating EAI

The EAI of the PSSDB and DPSSDB specimens are shown in Figure 21 and Table 1. The PSSDB-H specimens with unfilled PSS ribs achieved an EAI value of 396 kN.mm, which enhanced slightly to 544 kN.mm (1.37 times) when employed infill concrete (PSSDB-NC). The enhancement was due to the improved bending strength and ductility of the specimens. However, the DPSSDB-F0 has achieved a major increase in EAI value of 1342 kN.mm (3.38 times), while the DPSSDB-P while partially infilled material obtained EAI equal to 1084 kN.mm (2.73 times). However, the EAI values of all specimens decreased slightly as the recycled aggregate content (EPS, CRCA, and CRFA) increased, which is logical considering the impact of the reduced compressive strength of the concrete mixture (see Figure 21). In general, the contribution and high-energy absorption performance were achieved and recorded for the DPSSDB specimen with full and partially full PSS. However, the EAI values and percentages of increments varied, as shown in Figure 21.

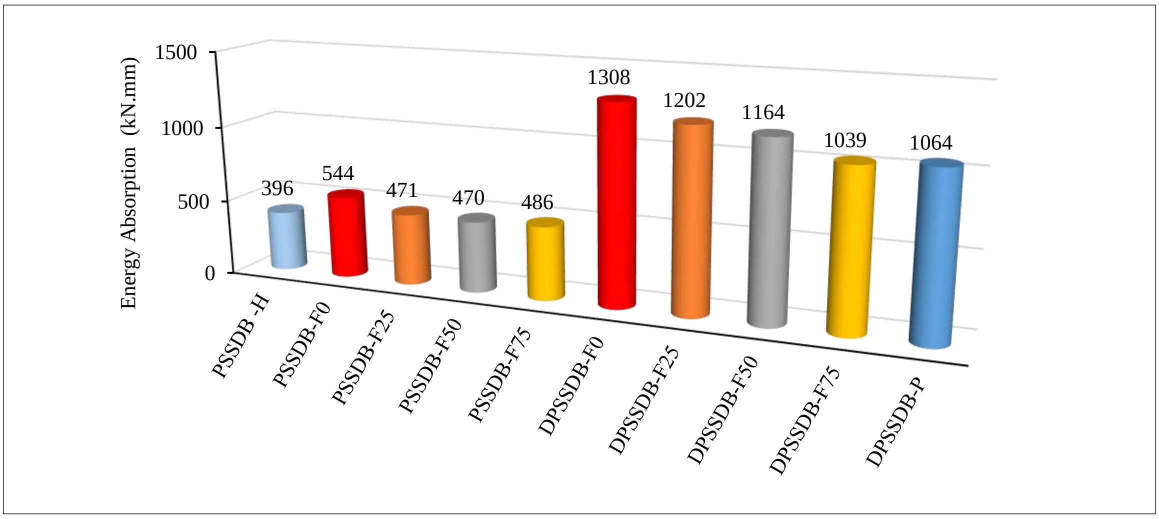

Figure 21. The EAI values of slab specimens

4. Development of A New Theoretical Model

Cold-formed light-gauge profile steel sheet sections can be categorized into three groups based on their buckling behavior under compressive stress when subjected to flexural loads: compact, noncompact (semi compact), and slender sections [29, 47]. According to Section B4 of the ANSI/AISC A360-16 standards, the proposed DPSSDB specimen, fabricated using double PSS sections filled with concrete, was classified as a slender section. The PSS top flange exhibited buckling under compressive stress at the midspan above the NA, which is indicative of the relatively small depth of the PSS compared with its cross-sectional dimensions.

Currently, no analytical model can accurately predict the nominal bending moment capacity (M_n) of the composite DPSSDB slab members. Therefore, this study involved the development of a novel theoretical framework based on the stress-block theory, as illustrated in Figure 22. The key assumptions for developing this model are as follows:

- The model was specifically designed for a DPSSDB composite slab system filled with concrete, constructed using double PSS (Peva 50) sections connected to a dry board sheet (DB; type: Prima*flex*), and subjected to four-point bending static loads.

- No slip failures were observed in the experimental results for the DPSSDB slab owing to the perfect connection between the PSS grooves with the concrete surface core (as discussed in the failure mode Section 3.1).
- The infill concrete portions below the NA were not considered in the investigation because they were subjected to tensile stress and exhibited cracking failure.
- The DPSSDB slab was considered a slender section and pure elastic behavior was assumed for these sections. This behavior was limited to the yield strength (*fy-pss*) at the bottom flange of the PSS, where the maximum tensile stress occurred, as indicated by the tensile strain values in Figure 18 (SG5). The maximum compressive stress at the top flange of the PSS was restricted to the buckling stress (*fs-pss*), because the stress did not reach the yield limit (refer to SG2-DPSSDB in Figure 18). Therefore, linear interpolation was employed to estimate the *fs-pss* value based on the *fy-pss* value.
- As discussed in the failure mode Section 3.1, the compressive stress was reduced to 80% of the maximum value for the concrete infill and DB sheet, due to the absence of crush failure observed in these components during testing.
- For practicality and model simplicity, the position of the NA. (*Yn*) is assumed to be at the mid-height of the upper PSS web, based on the reading of SG3-DPSSDB, as discussed in section 3.3 (moment–strain gauge relationship) and shown in Figure 18.
- Finally, a reduction factor (Ø) of 0.8 is assumed for design purposes to predict the Mn value of all DPSSDB specimens fully filled with normal and recycled concrete and partially filled with normal concrete.

$$ØMn = Ø(Mn_{pss\text{-}comp.} + Mn_{con} + Mn_{DB} + Mn_{pss\text{-}ten.}) \tag{1}$$

$$Mn_{pss\text{-}comp.} = F_{pss\text{-}c\text{-}flange} \cdot Y_{pss\text{-}c\text{-}flange} + F_{pss\text{-}c\text{-}web} \cdot Y_{pss\text{-}c\text{-}web} \tag{2}$$

$$Mn_{con} = F_{con} \cdot Y_{con} \tag{3}$$

$$Mn_{DB} = F_{DB} \cdot Y_{DB} \tag{4}$$

$$Mn_{pss\text{-}ten.} = F_{pss\text{-}t\text{-}top\ web} \cdot Y_{pss\text{-}t\text{-}top\ web} + F_{pss\text{-}t\text{-}top\ flange} \cdot Y_{pss\text{-}t\text{-}top.flange} + F_{pss\text{-}t\text{-}bot.web} \cdot Y_{pss\text{-}t\text{-}bot\ web} + F_{pss\text{-}t\text{-}bot.flange} \cdot Y_{pss\text{-}t\text{-}bot.flange} \tag{5}$$

Substituting Equations 2 to 5 into Equation 1 to calculate *ØMn*.

The details of the forces (*F*) and arm distance from the NA (*Yn*) are as follows:

$F_{pss\text{-}c\text{-}flange}$	$= f_{s\text{-}pss} \cdot A_{pss\text{-}flange}$	$= f_{s\text{-}pss} \cdot (3W_{pss} \cdot t_{pss})$
$F_{pss\text{-}c\text{-}web}$	$= f_{s\text{-}pss} \cdot A_{pss\text{-}web}$	$= f_{s\text{-}pss} \cdot 6\,(0.5 \cdot 1.2D_{pss} \cdot t_{pss})$
F_{con}		$= 0.8f_{cu} \cdot 5(0.5A_{rib\text{-}con})$
F_{DB}		$= 0.8f_{u\text{-}DB} \cdot (b_{eff} \cdot t_{DB})$
$F_{pss\text{-}t\text{-}top\ web}$	$= f_{y\text{-}pss} \cdot A_{pss\text{-}top\ web}$	$= f_{y\text{-}pss} \cdot 6(1.2D_{pss} \cdot t_{pss})$
$F_{pss\text{-}t\text{-}top\ flange}$	$= f_{y\text{-}pss} \cdot A_{pss\text{-}top.flange}$	$= f_{y\text{-}pss} \cdot 5(W_{pss} \cdot t_{pss})$
$F_{pss\text{-}t\text{-}web}$	$= f_{y\text{-}pss} \cdot A_{pss\text{-}web}$	$= f_{y\text{-}pss} \cdot 4(1.2D_{pss} \cdot t_{pss})$
$F_{pss\text{-}t\text{-}bot.\ flange}$	$= f_{y\text{-}pss} \cdot A_{pss\text{-}bot.flange}$	$= f_{y\text{-}pss} \cdot 2(W_{pss} \cdot t_{pss})$
$Y_{pss\text{-}c\text{-}flange}$	= distance between $F_{pss\text{-}c\text{-}flange}$ and NA.	$= 1/2\ D_{pss} + 1/2t_{pss}$
$Y_{pss\text{-}c\text{-}web}$	= distance between $F_{pss\text{-}c\text{-}web}$ and NA.	$= 1/4\ D_{pss}$
Y_{con}	= distance between F_{con} and NA.	$= 1/4\ D_{pss}$
Y_{DB}	= distance between F_{DB} and NA.	$= 1/2\ D_{pss} + 1/2t_{DB}$
$Y_{pss\text{-}t\text{-}top\ web}$	= distance between $F_{pss\text{-}t\text{-}top\ web}$ and NA.	$= 1/4\ D_{pss}$
$Y_{pss\text{-}t\text{-}top\ flange}$	= distance between $F_{pss\text{-}t\text{-}top\ flange}$ and NA.	$= 1/2D_{pss} + 1/2t_{pss}$
$Y_{pss\text{-}t\text{-}web}$	= distance between $F_{pss\text{-}t\text{-}web}$ and NA.	$= D_{pss}$
$Y_{pss\text{-}t\text{-}bot.\ flange}$	=distance between $F_{pss\text{-}t\text{-}bot.\ flange}$ and NA.	$= 3/2\ D_{pss} + 1/2\ t_{pss}$

Ø = 0.8 for all the DPSSDB specimens.

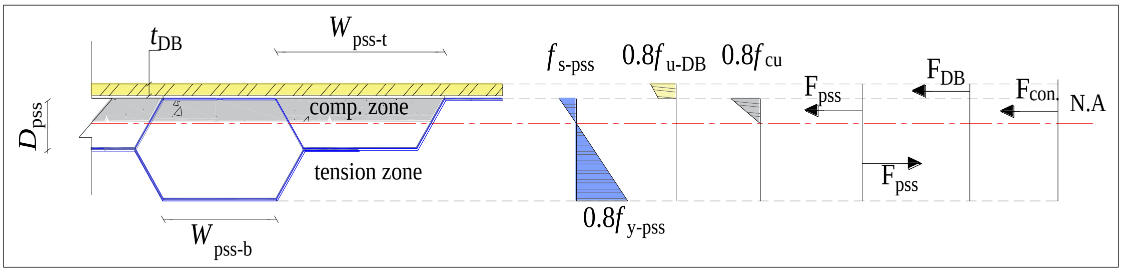

Figure 22. Stress block diagram for the slender composite DPSSDB slab section

The new analytical model was employed to predict the *Mn* capacity for the DPSSDB specimens under two-point load then compared with results collected from the experimental test. The comparison between the ultimate moment (*Mu*) and the nominal moment (*ØMn*) shown in Figure 23. The derived model achieved acceptable standard deviations and mean values equal to 8.1% and 0.965, respectively.

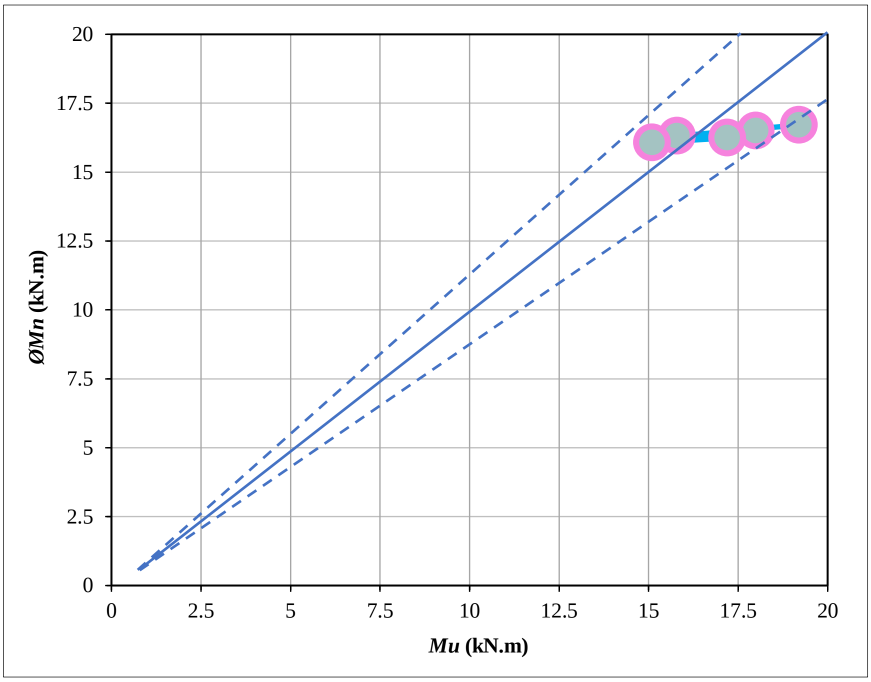

Figure 23. The comparison between the ultimate moment (*Mu*) and the nominal moment (*ØMn*)

5. Conclusions

The flexural performance of a newly proposed composite slab system, consisting of a double profile steel sheet and dry board (DPSSDB) filled with various types of concrete materials (normal and recycled), was experimentally investigated under a four-point static load. The key conclusions are summarized as follows:

- ***Enhanced Performance with Normal Concrete***: Filling the PSSDB composite slab system with normal concrete (0% replacement aggregates) significantly improved bending strength and energy absorption index (EAI) by approximately 14.5% and 37.3%, respectively, compared to the hollow specimen (PSSDB-H). When the PSSDB was filled with concrete containing 25%, 50%, and 75% replaced recycled aggregates, the bending moment increased by 12.9%, 11.2%, and 9.6%, respectively, and the EAI improved by 31%, 23%, and 21%, respectively.
- ***Perfect Bond Interaction***: Both the PSSDB and DPSSDB slabs demonstrated perfect bond interactions between their components when connected using steel self-tapping screws. No slip failures were recorded in the concrete core of the DPSSDB, even under extreme loading. Additionally, no crack failures were observed in the concrete core up to a maximum deflection of Le/50, except for slight cracks in the DPSSDB specimens under point loads beyond the extreme loading point.
- ***Improved Flexural Performance***: The addition of extra PSS components to the PSSDB slab system, resulting in the DPSSDB, significantly enhanced the flexural performance, including bending moment capacity, EAI, and ductility under static bending loads. Specifically, filling the DPSSDB-F0 slab with normal concrete increased the bending capacity by approximately 170% compared to the single PSS part slab (PSSDB-F0), while the self-weight increased by only 80%.

- ***Impact of Recycled Aggregates*****:** Filling the PSSDB and DPSSDB specimens with concrete containing 25%, 50%, and 75% recycled aggregates resulted in similar bending behavior with a slight reduction in bending capacity, ranging from 6.5% to 20%, compared to the corresponding specimen filled with normal concrete (0% lightweight recycled aggregates). The use of multiple lightweight recycled aggregates (two sizes of crumb rubbers and EPS) in the concrete mixture provided two key benefits: contributing to sustainability goals and reducing the overall self-weight by 6% to 15%.
- ***Development of a Theoretical Model*****:** A novel theoretical model was developed to predict the nominal bending moment (Mn) for the composite DPSSDB slab under four-point bending loads. Using experimental results (moment vs. strain relationship), the neutral axis (NA) level was determined, and the stress block method was employed, achieving acceptable moment mean values and a standard deviation of 0.965 and 8.1%, respectively.
- ***Future Research Needs*****:** Further experimental and numerical research is necessary to investigate different parameters and loading conditions for this new composite DPSSDB slab system, including the adoption of different types of profiled steel sheets and dry boards and testing the slab system under fatigue, cyclic, and long-term loading scenarios

6. Nomenclature

$Ø$	Reduction factor
A_{pss}	Area of the PSS cross-section
b_{eff}	Effective width of the DB
CA	Coarse Aggregate
CRA	Crumb rubber aggregate
DB	Dry board
D_{pss}	Depth of the PSS
DPSSDB	Double profile steel sheet dry board
EAI	Energy absorption index
E_c	Modulus of elasticity for concrete
EPS	Expanded polystyrene beads
E_s	Modulus of elasticity for steel
FA	Fine aggregate
F_{con}	Force on concrete part inside the PSS
f_{cu}	Compressive strength of concrete
F_{DB}	Force on the DB
$F_{pss\text{-}c\text{-}flange}$	Force on the PSS's flange in compression zone
$F_{pss\text{-}c\text{-}web}$	Force on the PSS's web in compression zone
F0	Normal concrete 0% replacement aggregate
F25	Recycled concrete 25% replacement aggregate
F50	Recycled concrete 50% replacement aggregate
F75	Recycled concrete 75% replacement aggregate
$F_{pss\text{-}t\text{-}bot.web}$	Force on the PSS's bottom web in tension zone
$F_{pss\text{-}t\text{-}top\ web}$	Force on the PSS's top web in tension zone
$F_{pss\text{-}t\text{-}bot.flange}$	Force on the PSS's bottom flange in tension zone
$F_{pss\text{-}t\text{-}top\ flange}$	Force on the PSS's top flange in tension zone
$f_{s\text{-}pss}$	Actual tensile strength of PSS
$f_{u\text{-}DB}$	Ultimate tensile strength of DB
$f_{y\text{-}pss}$	Yield tensile strength of PSS
Le	Effective length span
LVDTs	Linear variable differential transformers
Mn	Nominal bending moment
Mu	Ultimate bending moment
PSS	Profile steel sheet
PSSDB	Profile steel sheet dry board slab
SD	Standard Deviation
SG	Strain gauge
t_{DB}	Thickness of DB
t_{pss}	Thickness of PSS
W_{pss}	The rib's width of the PSS

7. Declarations

7.1. Author Contributions

Conceptualization, A.S.Z.A., F.D., and A.W.A.Z.; data curation, A.S.Z.A., A.W.A.Z., and F.D.; formal analysis, A.S.Z.A., N.A.R., and M.C.L.; funding acquisition, A.S.Z.A., A.W.A.Z., and F.D.; investigation, A.S.Z.A. and F.D.; methodology, F.D. and A.W.A.Z.; project administration A.S.Z.A., F.D., N.A.R., and A.W.A.Z.; validation, A.S.Z.A., F.D. and A.W.A.Z.; resources, A.W.A.Z., A.S.Z.A., and F.D.; software, A.W.A.Z. and A.S.Z.A.; supervision, F.D., A.W.A.Z., and N.A.R.; visualization, M.C.L., A.W.A.Z., and A.S.Z.A.; writing—original draft, A.S.Z.A., A.W.A.Z., and F.D.; writing—review & editing, F.D., A.W.A.Z., N.A.R., and M.C.L. All authors have read and agreed to the published version of the manuscript.

7.2. Data Availability Statement

The data presented in this study are available in the article.

7.3. Funding

This research was funded by a University Sains Malaysia (USM), Bridging Grant with Project No: R501-LR-RND003-0000000740-0000.

7.4. Acknowledgments

The authors acknowledge and appreciate the support of School of Civil Engineering, Universiti Sains Malaysia (USM), and Department of Civil Engineering, Universiti Kebangsaan Malaysia (UKM).

7.5. Conflicts of Interest

The authors declare no conflict of interest.

8. References

[1] Wright, H. D., Evans, H. R., & Burt, C. A. (1989). Profiled steel sheet/dry boarding composite floors. Structural (The) engineer. Part A: the Journal of the Institution of Structural Engineers-monthly, 67(7), 114-120.

[2] Ahmed, E., Wan Badaruzzaman, W. H., & Wright, H. D. (2002). Two-way bending behavior of profiled steel sheet dry board composite panel system. Thin-Walled Structures, 40(11), 971–990. doi:10.1016/s0263-8231(02)00039-3.

[3] Wan Badaruzzaman, W. H., Zain, M. F. M., Akhand, A. M., & Ahmed, E. (2003). Dry boards as load bearing element in the profiled steel sheet dry board floor panel system - Structural performance and applications. Construction and Building Materials, 17(4), 289–297. doi:10.1016/S0950-0618(02)00105-8.

[4] Ahmed, E., Wan Badaruzzaman, W. H., & Wright, H. D. (2000). Experimental and finite element study of profiled steel sheet dry board folded plate structures. Thin-Walled Structures, 38(2), 125–143. doi:10.1016/S0263-8231(00)00039-2.

[5] Wan Badaruzzaman, W. H., & Ahmed, E. (2003). Finite Element Prediction of the Behavior of Profiled Steel Sheet Dry Board Folded Plate Structures an Improved Model (Research Note). International Journal of Engineering, 16(1), 21-32.

[6] Ahmed, E., & Badaruzzaman, W. H. W. (2013). Vibration performance of Profiled Steel Sheet Dry Board composite floor panel. KSCE Journal of Civil Engineering, 17(1), 133–138. doi:10.1007/s12205-013-1114-2.

[7] Wan Badaruzzaman, W. H., Zain, M. F. M., Shodiq, H. M., Akhand, A. M., & Sahari, J. (2003). Fire resistance performance of profiled steel sheet dry board (PSSDB) flooring panel system. Building and Environment, 38(7), 907–912. doi:10.1016/S0360-1323(03)00029-5.

[8] Al-Shaikhli, M. S., Wan Badaruzzaman, W. H., Baharom, S., & Al-Zand, A. W. (2017). The two-way flexural performance of the PSSDB floor system with infill material. Journal of Constructional Steel Research, 138, 79–92. doi:10.1016/j.jcsr.2017.06.039.

[9] Sutiman, N. A., Majid, M. A., Jaini, Z. M., & Roslan, A. S. (2021). Structural Behavior of Lightweight Composite Slab System. International Journal of Integrated Engineering, 13(3), 57–65. doi:10.30880/ijie.2021.13.03.007.

[10] Sarina Ismail, R. A. Z. A. (2017). Finite Element Modeling and Analysis of Sandwich Dry Floor Slab. International Journal of Civil & Environmental Engineering, 17(1), 1-26.

[11] Rahmadi, A. P., Wan Badaruzzaman, W. H., & Arifin, A. K. (2013). Prediction of deflection of the composite profiled steel sheet MDF-board (PSSMDFB) floor system. Procedia Engineering, 54, 457–464. doi:10.1016/j.proeng.2013.03.041.

[12] Gandomkar, F. A., Badaruzzaman, W. H. W., & Osman, S. A. (2012). Dynamic response of low frequency Profiled Steel Sheet Dry Board with Concrete infill (PSSDBC) floor system under human walking load. Latin American Journal of Solids and Structures, 9(1), 21–41. doi:10.1590/s1679-78252012000100002.

[13] Gandomkar, F. A., Wan Badaruzzaman, W. H., Osman, S. A., & Ismail, A. (2013). Experimental and numerical investigation of the natural frequencies of the composite profiled steel sheet dry board (PSSDB) system. Journal of the South African Institution of Civil Engineering, 55(1), 11–21.

[14] Bavan, M., & Bin Baharom, S. (2014). Improvement of Ultimate Strength of Continuous Profiled Steel Sheet Dry Board (PSSDB) Floor Slab. The International Conference on Civil and Architecture Engineering, 10(10), 1–1. doi:10.21608/iccae.2014.44200.

[15] Jaffar, M. I., Badaruzzaman, W. W., Abdullah, M. A. B., Baharom, S., Moga, L. G., & Sandu, A. V. (2015). Relationship between panel stiffness and mid-span deflection in Profiled steel sheeting dry board with geopolymer concrete infill. Materiale Plastice, 52(2), 243-248.

[16] Jaffar, M. I., Wan Badaruzzaman, W. H., Al Bakri Abdullah, M. M., Kamarulzaman, K., & Seraji, M. (2015). Effect of Geopolymer Concrete Infill on Profiled Steel Sheeting Half Dry Board (PSSHDB) Floor System Subjected to Bending Moment. Applied Mechanics and Materials, 754–755, 354–358. doi:10.4028/www.scientific.net/amm.754-755.354.

[17] Jaffar, M. I., Wan Badaruzzaman, W. H., & Baharom, S. (2016). Experimental tests on bending behavior of profiled steel sheeting dry board composite floor with geopolymer concrete infill. Latin American Journal of Solids and Structures, 13(2), 272–295. doi:10.1590/1679-78252028.

[18] Seraji, M., Wan Badaruzzaman, W. H., & Jaffar, M. I. (2015). Numerical Investigation on the Effect of Material Thicknesses on Membrane Action Development in PSSDB Floor System. 2nd International Conference on Geological and Civil Engineering, 10-11 January, 2015, Dubai, United Arab Emirates.

[19] Seraji, M., Badaruzzaman, W. H. W., & Osman, S. A. (2012). Experimental Study on the Compressive Membrane Action in Profiled Steel Sheet Dry Board (PSSDB) Floor System. International Journal on Advanced Science, Engineering and Information Technology, 2(2), 159. doi:10.18517/ijaseit.2.2.176.

[20] Gandomkar, F. A., Badruzzaman, W. H. W., Osman, S. A., & Ismail, I. (2013). Dynamic response of low frequency Profiled Steel Sheet Dry Board (PSSDB) floor system. Latin American Journal of Solids and Structures, 10(6), 1135–1154. doi:10.1590/S1679-78252013000600004.

[21] Gandomkar, F. A., Wan Badaruzzaman, W. H., & Osman, S. A. (2011). The natural frequencies of composite profiled steel sheet dry board with concrete infill (PSSDBC) system. Latin American Journal of Solids and Structures, 8(3), 351–372. doi:10.1590/S1679-78252011000300009.

[22] Roslan, A. S., Majid, M. A., Jaini, Z. M., Ismail, M. H., & Sutiman, N. A. (2022). A Preliminary Study on Vibration Response of Profiled Steel Sheet Dry Board (PSSDB) System under Heel-drop Test. International Journal of Integrated Engineering, 14(5), 114–121. doi:10.30880/ijie.2022.14.05.013.

[23] Gandomkar, F. A., Parsafar, S., Tosee, V. R., & Samimifard, N. (2021). Dynamic Behavior of Composite Floor Consisting Profiled Steel Sheet and Dry Board Under Explosion Load. Amirkabir Journal of Civil Engineering, 53(7), 633-636. doi:10.22060/ceej.2020.17546.6595.

[24] Kim, H. Y., & Jeong, Y. J. (2009). Steel-concrete composite bridge deck slab with profiled sheeting. Journal of Constructional Steel Research, 65(8–9), 1751–1762. doi:10.1016/j.jcsr.2009.04.016.

[25] Nakamura, S. I., Momiyama, Y., Hosaka, T., & Homma, K. (2002). New technologies of steel/concrete composite bridges. Journal of Constructional Steel Research, 58(1), 99–130. doi:10.1016/S0143-974X(01)00030-X.

[26] Han, L. H., Li, W., & Bjorhovde, R. (2014). Developments and advanced applications of concrete-filled steel tubular (CFST) structures: Members. Journal of Constructional Steel Research, 100, 211–228. doi:10.1016/j.jcsr.2014.04.016.

[27] Han, L. H., Yang, Y. F., & Tao, Z. (2003). Concrete-filled thin-walled steel SHS and RHS beam-columns subjected to cyclic loading. Thin-Walled Structures, 41(9), 801–833. doi:10.1016/S0263-8231(03)00030-2.

[28] Wang, W. H., Han, L. H., Li, W., & Jia, Y. H. (2014). Behavior of concrete-filled steel tubular stub columns and beams using dune sand as part of fine aggregate. Construction and Building Materials, 51, 352–363. doi:10.1016/j.conbuildmat.2013.10.049.

[29] Al Zand, A. W., Badaruzzaman, W. H. W., & Tawfeeq, W. M. (2020). New empirical methods for predicting flexural capacity and stiffness of CFST beam. Journal of Constructional Steel Research, 164, 105778. doi:10.1016/j.jcsr.2019.105778.

[30] Fang, C., Zhou, F., & Luo, C. (2018). Cold-formed stainless steel RHSs/SHSs under combined compression and cyclic bending. Journal of Constructional Steel Research, 141, 9–22. doi:10.1016/j.jcsr.2017.11.001.

[31] Al Zand, A. W., Wan Badaruzzaman, W. H., Ali, M. M., Hasan, Q. A., & Al-Shaikhli, M. S. (2020). Flexural performance of cold-formed square CFST beams strengthened with internal stiffeners. Steel and Composite Structures, 34(1), 123–139. doi:10.12989/scs.2020.34.1.123.

[32] Sifan, M., Gatheeshgar, P., Navaratnam, S., Nagaratnam, B., Poologanathan, K., Thamboo, J., & Suntharalingam, T. (2022). Flexural behaviour and design of hollow flange cold-formed steel beam filled with lightweight normal and lightweight high strength concrete. Journal of Building Engineering, 48, 103878. doi:10.1016/j.jobe.2021.103878.

[33] Liejy, M. C., Al Zand, A. W., Mutalib, A. A., Abdulhameed, A. A., Kaish, A. B. M. A., Tawfeeq, W. M., Baharom, S., Al-Attar, A. A., Hanoon, A. N., & Yaseen, Z. M. (2023). Prediction of the Bending Strength of a Composite Steel Beam–Slab Member Filled with Recycled Concrete. Materials, 16(7), 2748. doi:10.3390/ma16072748.

[34] Liejy, M. C., Al Zand, A. W., Mutalib, A. A., Alghaaeb, M. F., Abdulhameed, A. A., Al-Attar, A. A., Tawfeeq, W. M., & Hilo, S. J. (2023). Flexural Performance of a Novel Steel Cold-Formed Beam–PSSDB Slab Composite System Filled with Concrete Material. Buildings, 13(2), 432. doi:10.3390/buildings13020432.

[35] Abendeh, R., Ahmad, H. S., & Hunaiti, Y. M. (2016). Experimental studies on the behavior of concrete-filled steel tubes incorporating crumb rubber. Journal of Constructional Steel Research, 122, 251–260. doi:10.1016/j.jcsr.2016.03.022.

[36] Ataria, R. B., & Wang, Y. C. (2022). Mechanical Properties and Durability Performance of Recycled Aggregate Concrete Containing Crumb Rubber. Materials, 15(5), 1776. doi:10.3390/ma15051776.

[37] Alizadeh, M., Eftekhar, M. R., Asadi, P., & Mostofinejad, D. (2024). Enhancing the mechanical properties of crumb rubber concrete through polypropylene mixing via a pre-mixing technique. Case Studies in Construction Materials, 21, 3569. doi:10.1016/j.cscm.2024.e03569.

[38] Al Zand, A. W., Ali, M. M., Al-Ameri, R., Badaruzzaman, W. H. W., Tawfeeq, W. M., Hosseinpour, E., & Yaseen, Z. M. (2021). Flexural strength of internally stiffened tubular steel beam filled with recycled concrete materials. Materials, 14(21), 6334. doi:10.3390/ma14216334.

[39] D'Orazio, M., Stipa, P., Sabbatini, S., & Maracchini, G. (2020). Experimental investigation on the durability of a novel lightweight prefabricated reinforced-EPS based construction system. Construction and Building Materials, 252, 119134. doi:10.1016/j.conbuildmat.2020.119134.

[40] El Gamal, S., Al-Jardani, Y., Meddah, M. S., Abu Sohel, K., & Al-Saidy, A. (2024). Mechanical and thermal properties of lightweight concrete with recycled expanded polystyrene beads. European Journal of Environmental and Civil Engineering, 28(1), 80–94. doi:10.1080/19648189.2023.2200830.

[41] Shabbar, R., Almusawi, A. M., & Taher, J. K. (2024). Investigation into the mechanical and thermal properties of lightweight mortar using commercial beads or recycled expanded polystyrene. Open Engineering, 14(1), 20220592. doi:10.1515/eng-2022-0592.

[42] Al Zand, A. W., Alghaaeb, M. F., Liejy, M. C., Mutalib, A. A., & Al-Ameri, R. (2022). Stiffening Performance of Cold-Formed C-Section Beam Filled with Lightweight-Recycled Concrete Mixture. Materials, 15(9), 2982. doi:10.3390/ma15092982.

[43] Jaffar, M. I., Wan Badaruzzaman, W. H., Al Bakri Abdullah, M. M., & Abd Razak, R. (2015). Comparative Study Floor Flexural Behavior of Profiled Steel Sheeting Dry Board between Normal Concrete and Geopolymer Concrete In-Filled. Applied Mechanics and Materials, 754–755, 364–368. doi:10.4028/www.scientific.net/amm.754-755.364.

[44] ASTM E8/E8M-22. (2024). Standard Test Methods for Tension Testing of Metallic Materials. ASTM International, Pennsylvania, United States. doi:10.1520/E0008_E0008M-22.

[45] Al-Shaikhli, M. S., Badaruzzaman, W. H. W., & Al Zand, A. W. (2022). Experimental and numerical study on the PSSDB system as two-way floor units. Steel and Composite Structures, 42(1), 33–48. doi:10.12989/scs.2022.42.1.033.

[46] B.S 1881-116. (1983). Method for Determination of Compressive Strength of Concrete Cubes. British Standards Institution, London, United Kingdom.

[47] Lai, Z., Varma, A. H., & Zhang, K. (2014). Noncompact and slender rectangular CFT members: Experimental database, analysis, and design. Journal of Constructional Steel Research, 101, 455–468. doi:10.1016/j.jcsr.2014.06.004.